Hindawi
Structural Control and Health Monitoring
Volume 2023, Article ID 4752776, 33 pages
https://doi.org/10.1155/2023/4752776

*Research Article*

# Bayesian Vehicle Load Estimation, Vehicle Position Tracking, and Structural Identification for Bridges with Strain Measurement

**Ka-Veng Yuen**,[1,2] **Hou-Zuo Guo**,[1] **and He-Qing Mu**[3,4]

[1]*State Key Laboratory of Internet of Things for Smart City and Department of Civil and Environmental Engineering, University of Macau, Macao 999078, China*
[2]*Guangdong-Hong Kong-Macau Joint Laboratory for Smart Cities, University of Macau, Macao 999078, China*
[3]*School of Civil Engineering and Transportation, South China University of Technology, Guangzhou 510640, China*
[4]*State Key Laboratory of Subtropical Building and Urban Science, South China University of Technology, Guangzhou 510640, China*

Correspondence should be addressed to Ka-Veng Yuen; kvyuen@um.edu.mo

Received 3 May 2023; Revised 17 September 2023; Accepted 6 October 2023; Published 27 October 2023

Academic Editor: Tzu-Kang Lin



Vehicle load estimation and health monitoring of bridges are of great importance for the health monitoring of bridge structure under vehicle loads. Traditional methods for the estimation of vehicle load require the positions of the vehicles. The vehicle position tracking is generally conducted in offline manner and requires the installation of additional sensors. To resolve these problems, we developed a Bayesian probabilistic approach for the online estimation of vehicle loads, vehicle positions, and structural parameters for bridges. The crux is to model the vehicle load vector as a modulated filtered Gaussian white noise due to the fact that the vehicle-bridge interaction forces are in essence the responses of the vehicle-bridge coupled system under the excitation of the road roughness described by Gaussian random field and the constant vehicle weights. Furthermore, the vehicle speed vector is introduced to track the unknown positions of vehicles. There are three appealing features in this approach. First, it allows the simultaneous estimation of vehicle loads, vehicle positions, and structural parameters in an online manner. Second, this method allows for time-varying vehicle speed tracking. Third, the proposed method is applicable to the case with multiple vehicles. Examples for the case where single/multiple vehicles pass across bridges with uniform speeds/variable speeds are presented to demonstrate the feasibility of the proposed method for vehicle load estimation, vehicle position tracking, and bridge structural identification using only strain measurements.

## 1. Introduction

Health monitoring of bridge structures under vehicle loads has attracted great interest in recent decades [1–3]. As one of the major excitations of bridge structures, vehicle loads may result in damage or fatigue problems [4]. On the other hand, the load by overweight vehicles may lead to collapse. Therefore, vehicle load estimation and structural identification of bridges are important for the assessment and maintenance of the bridge structures under vehicle loads.

As vehicle loads are moving loads, two problems are involved in the identification of vehicle-bridge coupled system, namely, vehicle load estimation and vehicle position tracking. In most of the existing methods, accurate estimation of vehicle positions is the prerequisite for vehicle load estimation. Early works [5] regarding vehicle position tracking or axle detection have been conducted with the axle detector installed on bridge deck. However, this setting is not durable and its maintenance is difficult. To resolve this problem, the concept of nothing-on-road (NOR) [6] was then proposed for position tracking using global responses. O'Brien et al. [7] and Bao et al. [8] utilized shear strains for the estimation of vehicle position. Lydon et al. [9] estimated the vehicle position using fiber-optic sensors with bearing strain measurements. He et al. [10] developed a virtual simply-supported beam method to determine the vehicle position with flexural bending strains. Nevertheless, all of these methods are conducted in an offline manner. In

addition, these methods require the installation of additional sensors in addition to those for vehicle load estimation [11].

On the other hand, considerable efforts have been dedicated to the studies on vehicle load estimation with given vehicle positions. The reason is that the interactions between the vehicles and bridge structure result in the complex vehicle-bridge coupled vibration [12, 13], increasing the difficulty of the inverse problem. Static approaches [5, 14] were first proposed, but they are applicable only to some short-span bridges whose dynamic effect can be ignored. To this end, the moving force identification (MFI) methods [15–17] were developed by considering the dynamic responses of bridge structure under time-variant moving forces. On this basis, simultaneous estimation of vehicle loads and structural properties was achieved [18]. Although the vibration of bridge structure can be reflected in the MFI methods, simultaneous estimation of vehicle loads and bridge structural parameters from a limited number of response measurements is ill-posed. Therefore, additive regularizations [19, 20] are usually required in these methods. In addition, all the aforementioned methods are applied in an offline manner so they are inapplicable to real-time structural health monitoring.

To address the problems involved in the MFI methods, some researchers proposed to estimate the vehicle load based on vehicle-bridge interaction dynamics. With assumed road roughness of the bridge deck, Lalthlamuana and Talukdar [21] estimated the vehicle loads through the particle filter in conjunction with the solution to vehicle-bridge interaction problem. By use of a sensor-equipped vehicle, Wang et al. [22] estimated the road roughness. The estimated roughness was then incorporated into the particle filter for the determination of vehicle loads under general traffic. Additional information of road roughness and vehicle parameters are generally required in these methods but they are difficult to be accurately estimated. To avoid the direct analysis of the coupled system, Wang et al. [23] introduced the random walk model [24] for vehicle loads and conducted the simultaneous estimation of the vehicle loads and bridge states with augmented Kalman filter (AKF). Lai et al. [25] further achieved the estimation of structural parameters with model updating method. However, there are errors in the estimation with random walk vehicle load model. The online estimation of vehicle loads and bridge structure is still unavailable.

More recently, Ojio et al. [26] proposed the concept of contactless bridge-weigh-in-motion (BWIM), which conducted the estimation of vehicle loads and vehicle positions through computer vision. Lansdell et al. [27] developed a speed correction procedure for static BWIM to consider the estimation of the bridge under speed varying traffic. Chen et al. [28] developed a BWIM system to measure the speed, wheelbase, and axial and gross weight of vehicle using a set of long-gauge fiber Bragg grating sensors without additional devices. This method was then extended to the case with the passage of multiple vehicles [29]. More literatures about the recent development of the estimation of vehicle loads and vehicle positions can be found in [20, 30–35]. However, to the best knowledge of the authors, there has been no report on the simultaneous estimation of vehicle loads, vehicle positions, and structural parameters for bridge structures, especially in an online manner.

In this paper, a Bayesian probabilistic approach is presented for the real-time simultaneous estimation of vehicle loads, vehicle positions, and bridge structure using strain measurements. The rest of the paper is organized as follows. In Section 2, the interaction dynamics of vehicle-bridge coupled system is introduced. In Section 3, the proposed method is presented. First, the modelling of vehicle loads and vehicle positions is introduced. Then, an augmented state space equation for vehicle load, vehicle position, and bridge structure is established. Thereafter, the estimation scheme with extended Kalman filter (EKF) is presented and supplementary constraints for vehicle load estimation and position tracking are presented. Finally, the procedure of the proposed algorithm is summarized in Section 4. In Section 5, two illustrated examples with a single-span bridge and a multispan bridge under different vehicle passing cases are presented to demonstrate the feasibility of the proposed method.

## 2. Vehicle-Bridge Interaction Dynamics

Figure 1 shows a schematic diagram of a bridge model with the passage of multiple vehicles and it illustrates the formulation of the vehicle-bridge coupled system [36].

The equation of motion for the vehicles can be expressed as follows:

$$\mathbf{M}_v^{(k)}\ddot{\mathbf{Y}}_v^{(k)}(t) + \mathbf{C}_v^{(k)}\dot{\mathbf{Y}}_v^{(k)}(t) + \mathbf{K}_v^{(k)}\mathbf{Y}_v^{(k)}(t) = \mathbf{L}_v^{(k)}\left[F^{(k)}(t) - G^{(k)}\right], \quad (k = 1, 2, \ldots, N_v), \tag{1}$$

where $\mathbf{M}_v^{(k)}$, $\mathbf{C}_v^{(k)}$, and $\mathbf{K}_v^{(k)}$ are the mass, damping, and stiffness matrix of the $k$-th vehicle, respectively; $\mathbf{Y}_v^{(k)}$, $\dot{\mathbf{Y}}_v^{(k)}$, and $\ddot{\mathbf{Y}}_v^{(k)}$ are, respectively, the displacement, velocity, and acceleration vector of the $k$-th vehicle with respect to its static equilibrium position under the vehicle weight; $F^{(k)}$ and $G^{(k)}$ are the vehicle-bridge interaction force and the vehicle weight of the $k$-th vehicle, respectively; $\mathbf{L}_v^{(k)}$ is the location vector of $F^{(k)}(t) - G^{(k)}$ for the vehicle; and $N_v$ is the number of vehicles on the bridge.

The equation of motion for the bridge structure can be expressed as follows:

$$\mathbf{M}_b\ddot{\mathbf{Y}}_b(t) + \mathbf{C}_b\left[\boldsymbol{\theta}_{\mathbf{C}}(t)\right]\dot{\mathbf{Y}}_b(t) + \mathbf{K}_b\left[\boldsymbol{\theta}_{\mathbf{K}}(t)\right]\mathbf{Y}_b(t) = \mathbf{L}_b(\mathbf{x})\mathbf{F}(t), \tag{2}$$

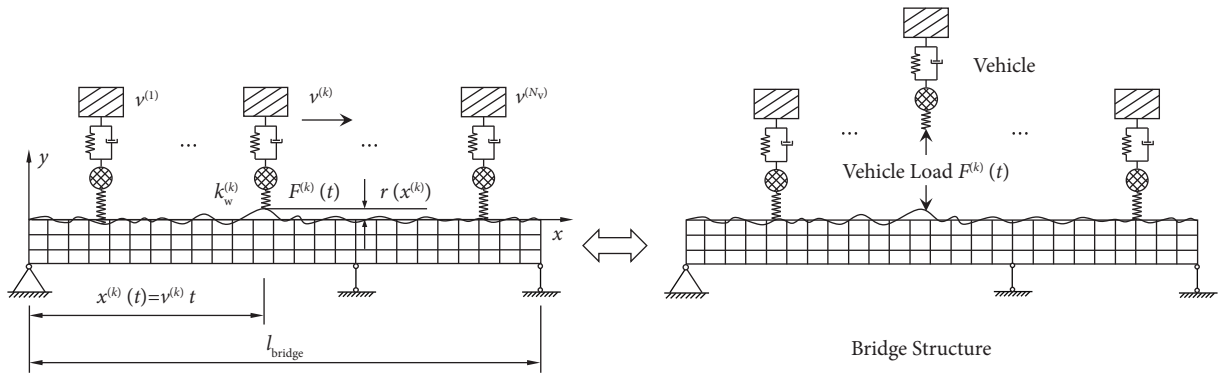


FIGURE 1: Multiple vehicles passing across the bridge.

where $\mathbf{M}_b$, $\mathbf{C}_b$, and $\mathbf{K}_b$ are the mass, damping, and stiffness matrix of the bridge structure, respectively; $\theta_{\mathbf{C}}$ and $\theta_{\mathbf{K}}$ are the structural parameter vectors introduced to parameterize $\mathbf{C}_b$ and $\mathbf{K}_b$, respectively; $\mathbf{Y}_b$, $\dot{\mathbf{Y}}_b$, and $\ddot{\mathbf{Y}}_b$ are the displacement, velocity, and acceleration vector of the bridge structure, respectively; $\mathbf{F}(t) = [F^{(1)}(t), F^{(2)}(t), \cdots, F^{(N_v)}(t)]^{\mathrm{T}}$, where $F^{(k)}(t)$ is the vehicle-bridge interaction force of the $k$-th vehicle at time $t$; and $\mathbf{L}_b(\mathbf{x}) = [\mathbf{L}_b(x^{(1)}), \mathbf{L}_b(x^{(2)}), \cdots, \mathbf{L}_b(x^{(N_v)})]$, where $\mathbf{L}_b(x^{(k)})$ is the time-dependent location vector of $F^{(k)}(t)$ for the bridge structure, which is given by the following equation:

$$\mathbf{L}_b\left(x^{(k)}\right) = \begin{cases} \mathbf{L}_{b0}\left(x^{(k)}\right), & \text{when } 0 < x^{(k)} \le l_{\text{bridge}}, \\ \mathbf{0}, & \text{when } x^{(k)} \le 0 \text{ or } x^{(k)} > l_{\text{bridge}}, \end{cases} \quad (k = 1, 2, \ldots, N_v), \tag{3}$$

where $\mathbf{L}_{b0}(\cdot)$ is the location vector of loads; $x^{(k)} = x^{(k)}(t)$ is the position of the $k$-th vehicle on the bridge structure at time $t$; and $L_{\text{bridge}}$ is the total length of the bridge structure. Note that $\mathbf{L}_b(x^{(k)}) = \mathbf{0}$ when $x^{(k)} \le 0$ or $x^{(k)} > l_{\text{bridge}}$, this is because the $k$-th vehicle has not entered the bridge or has exited the bridge.

From the two sets of equations of motion in equations (1) and (2), the motions of the vehicles and the bridge structure are coupled via the interaction forces $F^{(k)}$ $(k = 1, 2, \ldots, N_v)$. The interaction forces $F^{(k)}$ $(k = 1, 2, \ldots, N_v)$ are modelled with the linear contact assumption [37], where the vehicles and the bridge structure are connected by elastic and tensionless springs. Specifically, the interaction force $F^{(k)}$ can be expressed as follows:

$$F^{(k)}(t) = \begin{cases} k_w^{(k)} \delta^{(k)}(t), & \text{when } \delta^{(k)}(t) > 0, \\ 0, & \text{when } \delta^{(k)}(t) \le 0, \end{cases} \quad (k = 1, 2, \ldots, N_v), \tag{4}$$

where $k_w^{(k)}$ is the stiffness of the connecting spring depending on the wheel type of the vehicle and $\delta^{(k)}$ is the total amount of the deformation of the connect spring as follows:

$$\delta^{(k)} = \left[y_d\left(x^{(k)}, t\right) - y_w^{(k)}(t) + r\left(x^{(k)}\right)\right] + y_{\text{st}}^{(k)} = \left[\mathbf{L}_b^T\left(x^{(k)}\right)\mathbf{Y}_b(t) - \mathbf{L}_v^T\mathbf{Y}_v^{(k)}(t) + r\left(x^{(k)}\right)\right] + y_{\text{st}}^{(k)}, \tag{5}$$

where $y_d(x^{(k)}, t)$ is the vertical displacement of the bridge deck at the contact point with the $k$-th vehicle at time $t$; $y_w^{(k)}(t)$ is the vertical displacement of the wheel of the $k$-th vehicle at time $t$; $r(\cdot)$ is the road roughness which is modelled as a zero-mean Gaussian random field; and $y_{\text{st}}^{(k)} = G^{(k)}/k_w^{(k)}$ is the vertical displacement of the wheel of the $k$-th vehicle under the vehicle weight. When $\delta^{(k)}(t) > 0$, the spring $k_w^{(k)}$ is in compression. When $\delta^{(k)}(t) \le 0$, there is no contact between the vehicle wheel and bridge deck, leading to zero contact force.

## 3. Estimation of Vehicle Loads and Bridge Structure

In this section, the modelling of vehicle loads and vehicle positions is introduced and then the vehicle load estimation, vehicle position tracking, and structural identification of bridges are conducted through the extended Kalman filter (EKF) technique.

*3.1. Modelling of Vehicle Loads and Vehicle Positions.* In the previous section, the equations of motion of vehicle-bridge coupled system are formulated and the expressions for vehicle loads are presented. As can be seen from equations (4) and (5), the vehicle loads, namely, the vehicle-bridge interaction forces, are in essence to the responses of the vehicle-bridge coupled system under the excitation of the road roughness described by Gaussian random field and the constant vehicle weights. From this point of view, a modulated filtered Gaussian white noise model, originally proposed for the excitation estimation of the structure under nonwhite noise ground motions [38, 39], is introduced in this study to model the vehicle load vector, which is given by the following equation:

$$\mathbf{F}(t) = \mathbf{P}(t) + \mathbf{G}, \tag{6}$$

where $\mathbf{F}(t) \in \mathbb{R}^{N_v \times 1}$ and $\mathbf{G} \in \mathbb{R}^{N_v \times 1}$ are, respectively, the vehicle load vector and vehicle weight vector with $N_v$ vehicles moving on the bridge; and $\mathbf{P}(t) \in \mathbb{R}^{N_v \times 1}$ is the dynamic component of vehicle load vector as follows:

$$\begin{aligned} \dot{\mathbf{y}}_f(t) &= \mathbf{A}_f\left[\boldsymbol{\theta}_f(t)\right]\mathbf{y}_f(t) + \mathbf{B}_f\mathbf{w}(t), \\ \mathbf{P}(t) &= \mathbf{C}_f\left[\boldsymbol{\theta}_f(t)\right]\mathbf{y}_f(t), \end{aligned} \tag{7}$$

where $\mathbf{y}_f(t) \in \mathbb{R}^{2N_v \times 1}$ is the internal filter state vector at time $t$; $\mathbf{w}$ is a $N_v$-variate zero-mean Gaussian white noise with covariance matrix $\boldsymbol{\Sigma}_{\mathbf{w}}(\boldsymbol{\psi}_{\mathbf{w}}(t))$; and $\mathbf{A}_f[\boldsymbol{\theta}_f(t)] \in \mathbb{R}^{2N_v \times 2N_v}$, $\mathbf{B}_f \in \mathbb{R}^{2N_v \times N_v}$, and $\mathbf{C}_f[\boldsymbol{\theta}_f(t)] \in \mathbb{R}^{N_v \times 2N_v}$ are the parameterized system matrices for the internal filter state as follows:

$$\begin{aligned} \mathbf{A}_f\left[\boldsymbol{\theta}_f(t)\right] &= \begin{bmatrix} 0 & 1 & 0 & 0 & \cdots & 0 & 0 \\ -\omega_1^2 & -2\xi_1\omega_1 & 0 & 0 & \cdots & 0 & 0 \\ 0 & 0 & 0 & 1 & \cdots & 0 & 0 \\ 0 & 0 & -\omega_2^2 & -2\xi_2\omega_2 & \cdots & 0 & 0 \\ \vdots & \vdots & \vdots & \vdots & \ddots & \vdots & \vdots \\ 0 & 0 & 0 & 0 & \cdots & 0 & 1 \\ 0 & 0 & 0 & 0 & \cdots & -\omega_{N_v}^2 & -2\xi_{N_v}\omega_{N_v} \end{bmatrix}, \\ \mathbf{B}_f &= \begin{bmatrix} 0 & 0 & \cdots & 0 \\ 1 & 0 & \cdots & 0 \\ 0 & 0 & \cdots & 0 \\ 0 & 1 & \cdots & 0 \\ \vdots & \vdots & \ddots & \vdots \\ 0 & 0 & \cdots & 0 \\ 0 & 0 & \cdots & 1 \end{bmatrix}, \\ \mathbf{C}_f\left[\boldsymbol{\theta}_f(t)\right] &= \begin{bmatrix} \omega_1^2 & 2\xi_1\omega_1 & 0 & 0 & \cdots & 0 & 0 \\ 0 & 0 & \omega_2^2 & 2\xi_2\omega_2 & \cdots & 0 & 0 \\ \vdots & \vdots & \vdots & \vdots & \ddots & \vdots & \vdots \\ 0 & 0 & 0 & 0 & \cdots & \omega_{N_v}^2 & 2\xi_{N_v}\omega_{N_v} \end{bmatrix}, \end{aligned} \tag{8}$$

where $\boldsymbol{\theta}_f = [\omega_1, \xi_1, \omega_2, \xi_2, \cdots, \omega_{N_v}, \xi_{N_v}]^T$ with $\omega_k, \xi_k$ ($k = 1, 2, \ldots, N_v$) being the characteristic filter parameters.

On the other hand, to track the vehicle positions, the time-varying vehicle speed vector $\mathbf{v}(t)$ is introduced. Then, the vehicle position vector $\mathbf{x}(t)$ can be modelled as follows:

$$\dot{\mathbf{x}}(t) = \mathbf{v}(t), \tag{9}$$

where $\mathbf{v}(t) = [v^{(1)}(t), v^{(2)}(t), \cdots, v^{(N_v)}(t)]^T$ with $v^{(k)}(t)$ being the speed of the $k$-th vehicle on the bridge structure at time $t$.

It should be noted that all the elements in $\mathbf{x}(t)$, $\mathbf{v}(t)$, and $\mathbf{F}(t)$ are, respectively, used to record the positions, speeds, and loads for the vehicles still moving on the bridge. When a vehicle, say the $k$-th vehicle, exits the bridge, the

corresponding elements, i.e., $x^{(k)}(t)$, $v^{(k)}(t)$, and $F^{(k)}(t)$, will be reset for the record of next vehicle.

*3.2. Formulation of Problem.* Introduce the augmented state vector $\mathbf{V}(t) = [\mathbf{y}_f^T(t), \mathbf{Y}_b^T(t), \dot{\mathbf{Y}}_b^T(t), \mathbf{x}^T(t), \mathbf{v}^T(t), \mathbf{G}^T(t), \boldsymbol{\theta}_f^T(t), \boldsymbol{\theta}_{\mathbf{K}}^T(t), \boldsymbol{\theta}_{\mathbf{C}}^T(t)]^T$, which includes the filtered state vector, the structural state vector, the vehicle position vector, vehicle speed vector, vehicle weight vector, the filter parameters, and the structural parameters. Then, based on equations (2), (7), and (9), the state space representation for the bridge structure under vehicle loads can be obtained as follows:

$$\dot{\mathbf{V}}(t) = \begin{bmatrix} \mathbf{A}_f\left[\boldsymbol{\theta}_f(t)\right]\mathbf{y}_f(t) + \mathbf{B}_f\mathbf{w}(t) \\ \dot{\mathbf{Y}}_b(t) \\ \mathbf{M}_b^{-1}\left\{-\mathbf{K}_b\left[\boldsymbol{\theta}_{\mathbf{K}}(t)\right]\mathbf{Y}_b(t) - \mathbf{C}_b\left[\boldsymbol{\theta}_{\mathbf{C}}(t)\right]\dot{\mathbf{Y}}_b(t) + \mathbf{L}_b[\mathbf{x}(t)]\mathbf{C}_f\left[\boldsymbol{\theta}_f(t)\right]\mathbf{y}_f(t) + \mathbf{L}_b[\mathbf{x}(t)]\mathbf{G}(t)\right\} \\ \mathbf{v}(t) \\ -\mu\mathbf{1}_{(4N_v+N_{\mathbf{K}}+N_{\mathbf{C}})\times 1} \end{bmatrix}, \tag{10}$$

where $\mathbf{Y}_b(t) \in \mathbb{R}^{N_d\times 1}$ and $\dot{\mathbf{Y}}_b(t) \in \mathbb{R}^{N_d\times 1}$ are the displacement and velocity vector of the bridge structure with $N_d$ being the number of degrees of freedom of the bridge structure; $\boldsymbol{\theta}_{\mathbf{K}}(t) \in \mathbb{R}^{N_{\mathbf{K}}\times 1}$ and $\boldsymbol{\theta}_{\mathbf{C}}(t) \in \mathbb{R}^{N_{\mathbf{C}}\times 1}$ are the structural parameter vectors with $N_{\mathbf{K}}$ and $N_{\mathbf{C}}$ being the number of stiffness parameters and damping parameters, respectively; $\mathbf{1}_{a\times 1}$ is the $a \times 1$ all-ones vector; and $\mu$ is a small positive number to avoid singularity in the calculation. By local linearization, equation (10) can be discretized as follows:

$$\mathbf{V}_{i+1} = \mathbf{A}_{\mathbf{V},i}\mathbf{V}_i + \mathbf{B}_{\mathbf{V}}\mathbf{w}_i + \mathbf{h}_i, \tag{11}$$

where $\mathbf{V}_i \equiv \mathbf{V}(t_i)$ and $\mathbf{w}_i \equiv \mathbf{w}(t_i)$, in which $t_i = i\Delta t$ with $\Delta t$ being the sampling time interval; $\mathbf{A}_{\mathbf{V},i}$ and $\mathbf{B}_{\mathbf{V}}$ are, respectively, the system matrix and the input matrix of the discretization of the state space representation in equation (10); and $\mathbf{h}_i$ is the intercept term in the Taylor's expansion.

The bridge responses are observed at $N_o$ DOFs with the sampling time step being $\Delta t$. The measurement can be written as follows:

$$\mathbf{z}_{i+1} = \mathbf{g}\left(\mathbf{V}_{i+1}\right) + \mathbf{n}_i, \tag{12}$$

where $\mathbf{z}_{i+1} \equiv \mathbf{z}(t_{i+1}) \in \mathbb{R}^{N_o\times 1}$; $\mathbf{g}(\cdot)$ is the observation function; and $\mathbf{n}_i \equiv \mathbf{n}(t_i) \in \mathbb{R}^{N_o\times 1}$ is the measurement noise modelled as a zero-mean Gaussian random vector with covariance matrix $\boldsymbol{\Sigma}_{\mathbf{n}}(\boldsymbol{\psi}_{\mathbf{n},i})$. Note that the strains can be expressed as function of the corresponding nodal displacements. Therefore, $\mathbf{z}_{i+1}$ in equation (12) can be strain measurements when the function $\mathbf{g}$ is properly chosen according to the positions.

*3.3. Estimation Scheme for Vehicle Load and Bridge Structure.* Use $\mathscr{D}_{1,i} = \{\mathbf{z}_1, \mathbf{z}_2, \cdots, \mathbf{z}_i\}$ to denote the response measurements up to the $i$-th time step. Then, based on equations (11) and (12), the posterior estimation of the augmented state vector and the corresponding covariance matrix can be obtained with EKF [40] as follows:

$$\mathbf{V}_{i+1|i} \equiv E\left(\mathbf{V}_{i+1} \mid \mathscr{D}_{1,i}\right) = \mathbf{A}_{\mathbf{V},i}\mathbf{V}_{i|i} + \mathbf{h}_i, \tag{13}$$

$$\boldsymbol{\Sigma}_{\mathbf{V},i+1|i} \equiv E\left[\left(\mathbf{V}_{i+1} - \mathbf{V}_{i+1|i}\right)\left(\mathbf{V}_{i+1} - \mathbf{V}_{i+1|i}\right)^T \mid \mathscr{D}_{1,i}\right] = \boldsymbol{\Lambda}\mathbf{A}_{\mathbf{V},i}\boldsymbol{\Sigma}_{\mathbf{V},i|i}\mathbf{A}_{\mathbf{V},i}^T\boldsymbol{\Lambda}^T + \mathbf{B}_{\mathbf{V}}\boldsymbol{\Sigma}_{\mathbf{w},i}\left(\boldsymbol{\psi}_{\mathbf{w},i}\right)\mathbf{B}_{\mathbf{V}}^T, \tag{14}$$

$$\mathbf{H}_{i+1} = \boldsymbol{\Sigma}_{\mathbf{V},i+1|i}\mathbf{C}_{\mathbf{V},i+1}^T\left[\mathbf{C}_{\mathbf{V},i+1}\boldsymbol{\Sigma}_{\mathbf{V},i+1|i}\mathbf{C}_{\mathbf{V},i+1}^T + \boldsymbol{\Sigma}_{\mathbf{n},i+1}\left(\boldsymbol{\psi}_{\mathbf{n},i+1}\right)\right]^{-1}, \tag{15}$$

$$\mathbf{V}_{i+1|i+1} = \mathbf{V}_{i+1|i} + \mathbf{H}_{i+1}\left(\mathbf{z}_{i+1} - \mathbf{C}_{\mathbf{V},i+1}\mathbf{V}_{i+1|i}\right), \tag{16}$$

$$\boldsymbol{\Sigma}_{\mathbf{V},i+1|i+1} = \left(\mathbf{I}_{7N_i+2N_d+N_{\mathbf{K}}+N_{\mathbf{C}}} - \mathbf{H}_{i+1}\mathbf{C}_{\mathbf{V},i+1}\right)\boldsymbol{\Sigma}_{\mathbf{V},i+1|i}, \tag{17}$$

where $\mathbf{V}_{i+1|i}$ and $\boldsymbol{\Sigma}_{\mathbf{V},i+1|i}$ are the predicted state vector and the corresponding covariance matrix, respectively; $\mathbf{V}_{i+1|i+1}$ and $\boldsymbol{\Sigma}_{\mathbf{V},i+1|i+1}$ are the filtered state vector and the corresponding covariance matrix, respectively; $\boldsymbol{\Lambda} = \mathrm{diag}[\mathbf{1}_{(2N_v+2N_d)\times 1}, \sqrt{\lambda_1}\cdot\mathbf{1}_{2N_v\times 1}, \sqrt{\lambda_2}\cdot\mathbf{1}_{N_v\times 1}, \sqrt{\lambda_3}\cdot\mathbf{1}_{(2N_v+N_{\mathbf{K}}+N_{\mathbf{C}})\times 1}]$ is a diagonal matrix with $\lambda_1$, $\lambda_2$, and $\lambda_3$ being the forgetting factors; $\mathbf{C}_{\mathbf{V},i+1}$ is the Jacobian matrix of the observation function $\mathbf{g}(\cdot)$; and $\mathbf{I}_a$ is the $a \times a$ identity matrix.

It is noted that the forgetting factors $\lambda_1, \lambda_2, \lambda_3 \geq 1$ are adopted to discount the contribution of the past data gradually so as to ensure the tracking capability of the filter for the time-varying parameters [41]. Literature regarding adaptive filtering techniques can be found in [42–44]. Since the identified values of the vehicle positions and vehicle speeds will change more rapidly than the model parameters of vehicle loads and the structural parameters of bridges, larger forgetting factors are used for $\lambda_1$ for the vehicle positions and vehicle speeds. Additionally, the entry of vehicles will lead to sudden increase of vehicle weights, and thus sufficiently large values are also required for $\lambda_2$ for the vehicle weights.

By now, the posterior estimation and posterior uncertainty of the augmented state vector can be obtained with the EKF shown in equations (13)–(17). Therefore, the concerned vehicle loads, vehicle positions, and structural parameters for the bridge included in the augmented state vector can be determined correspondingly.

*3.4. Estimation of Noise Parameters in EKF.* Since the performance of the EKF is affected by the noise covariance matrices $\boldsymbol{\Sigma}_{\mathbf{w}}(\boldsymbol{\psi}_{\mathbf{w}})$ and $\boldsymbol{\Sigma}_{\mathbf{n}}(\boldsymbol{\psi}_{\mathbf{n}})$ [45, 46], in this section, the noise parameters $\boldsymbol{\psi}_{\mathbf{w}}$ and $\boldsymbol{\psi}_{\mathbf{n}}$ for $\boldsymbol{\Sigma}_{\mathbf{w}}(\boldsymbol{\psi}_{\mathbf{w}})$ and $\boldsymbol{\Sigma}_{\mathbf{n}}(\boldsymbol{\psi}_{\mathbf{n}})$ shown in equations (14) and (15), respectively, are further estimated with the Bayesian methodology.

Define a noise parameter vector $\boldsymbol{\psi}_{i+1} = [\boldsymbol{\psi}_{\mathbf{w},i}^{\mathrm{T}}, \boldsymbol{\psi}_{\mathbf{n},i+1}^{\mathrm{T}}]^{\mathrm{T}}$. By use of the Bayes' theorem, the posterior PDF of $\boldsymbol{\psi}_{i+1}$ given the measurement $\mathscr{D}_{1,i+1}$ can be expressed as follows:

$$p\left(\boldsymbol{\psi}_{i+1} \mid \mathscr{D}_{1,i+1}\right) = c_0 p\left(\boldsymbol{\psi}_{i+1} \mid \mathscr{D}_{1,i}\right) p\left(\mathbf{z}_{i+1} \mid \boldsymbol{\psi}_{i+1}, \mathscr{D}_{1,i}\right), \tag{18}$$

where $p(\boldsymbol{\psi}_{i+1} \mid \mathscr{D}_{1,i})$ is the prior PDF of $\boldsymbol{\psi}_{i+1}$; $p(\mathbf{z}_{i+1} \mid \boldsymbol{\psi}_{i+1}, \mathscr{D}_{1,i})$ is the likelihood function; $c_0$ is the normalizing constant such that the integrating of $p(\boldsymbol{\psi}_{i+1} \mid \mathscr{D}_{1,i})$ over the domain of $\boldsymbol{\psi}_{i+1}$ yields unity. Considering the continuity of the noise parameters, the prior PDF $p(\boldsymbol{\psi}_{i+1} \mid \mathscr{D}_{1,i})$ can be approximated as a Gaussian distribution with $p(\boldsymbol{\psi}_{i+1} \mid \mathscr{D}_{1,i}) = \mathcal{N}(\boldsymbol{\psi}_{i \mid i}, \lambda_4 \boldsymbol{\Sigma}_{\boldsymbol{\psi},i \mid i})$, where $\lambda_4$ is the forgetting factor for the estimation of noise parameter vector. The likelihood function $p(\mathbf{z}_{i+1} \mid \boldsymbol{\psi}_{i+1}, \mathscr{D}_{1,i})$, formulated based on equations (12)–(14), can be expressed as follows:

$$p\left(\mathbf{z}_{i+1} \mid \boldsymbol{\psi}_{i+1}, \mathscr{D}_{1,i}\right) = (2\pi)^{-N_o/2} \left|\boldsymbol{\Sigma}_{\mathbf{z},i+1 \mid i}\right|^{-1/2} \exp\left[-\frac{1}{2}\left(\mathbf{z}_{i+1} - \mathbf{z}_{i+1 \mid i}\right)^T \boldsymbol{\Sigma}_{\mathbf{z},i+1 \mid i-1}\left(\mathbf{z}_{i+1} - \mathbf{z}_{i+1 \mid i}\right)\right], \tag{19}$$

where $\mathbf{z}_{i+1|i} = \mathbf{C}_{\mathbf{V},i+1}\mathbf{V}_{i+1|i}$ and $\boldsymbol{\Sigma}_{\mathbf{z},i+1|i} = \mathbf{C}_{\mathbf{V},i+1}\boldsymbol{\Lambda}\mathbf{A}_{\mathbf{V},i}\boldsymbol{\Sigma}_{\mathbf{V},i|i}\mathbf{A}_{\mathbf{V},i}^T \boldsymbol{\Lambda}^T\mathbf{C}_{\mathbf{V},i+1}^T + \mathbf{C}_{\mathbf{V},i+1}\mathbf{B}_{\mathbf{V}}\boldsymbol{\Sigma}_{\mathbf{w},i}\mathbf{B}_{\mathbf{V}}^T\mathbf{C}_{\mathbf{V},i+1}^T + \boldsymbol{\Sigma}_{\mathbf{n},i+1}$.

The objective function for $\boldsymbol{\psi}_{i+1}$ is defined as the negative logarithm of the posterior PDF $p(\boldsymbol{\psi}_{i+1} \mid \mathscr{D}_{1,i+1})$ as follows:

$$\begin{aligned} J(\boldsymbol{\psi}_{i+1}) &= -\ln\left[p\left(\boldsymbol{\psi}_{i+1} \mid \mathscr{D}_{1,i+1}\right)\right] \\ &= c_0 + \frac{1}{2}\ln\left|\sum_{\mathbf{z},i+1 \mid i}\right| + \frac{1}{2\lambda_4}\left(\boldsymbol{\psi}_{i+1} - \boldsymbol{\psi}_{i+1 \mid i}\right)^T \boldsymbol{\Sigma}_{\boldsymbol{\psi},i|i-1}\left(\boldsymbol{\psi}_{i+1} - \boldsymbol{\psi}_{i+1 \mid i}\right) + \frac{1}{2}\left(\mathbf{z}_{i+1} - \mathbf{z}_{i+1 \mid i}\right)^T \boldsymbol{\Sigma}_{\mathbf{z},i+1|i-1}\left(\mathbf{z}_{i+1} - \mathbf{z}_{i+1 \mid i}\right). \end{aligned} \tag{20}$$

The constant term $c_0 = [(N_V + 2N_o)\ln(2\pi) + 2\ln p(\mathbf{z}_{i+1} \mid D_{1,i}) + \ln|\lambda_4 \Sigma_{\boldsymbol{\psi},i \mid i}|]/2$ is excluded since it does not affect the optimization of $\boldsymbol{\psi}_{i+1}$. Then, the estimation of the noise parameter vector $\boldsymbol{\psi}_{i+1}$ can be obtained as follows:

$$\boldsymbol{\psi}_{i+1|i+1} = \arg\min_{\boldsymbol{\psi}_{i+1}}\left[J(\boldsymbol{\psi}_{i+1})\right]. \tag{21}$$

The covariance matrix of $\boldsymbol{\psi}_{i+1|i+1}$ can be determined by the inverse of the Hessian matrix as follows:

$$\boldsymbol{\Sigma}_{\boldsymbol{\psi},i+1|i+1} = \left[\mathbf{H}_J\left(\boldsymbol{\psi}_{i+1 \mid i+1}\right)\right]^{-1}, \tag{22}$$

where $\mathbf{H}_J(\boldsymbol{\psi}_{i+1 \mid i+1})$ is the Hessian matrix, given by $\mathbf{H}_J(\boldsymbol{\psi}_{i+1 \mid i+1}) = \nabla J(\boldsymbol{\psi}_{i+1}) \nabla^T|_{\boldsymbol{\psi}=\boldsymbol{\psi}_{i+1|i+1}}$. There is no closed-form solution for the optimization problem shown in equation (21), and thus the optimal noise parameter vector needs to be determined through the numerical optimization scheme presented in [45].

*3.5. Supplementary Constraints for Vehicle Load Estimation and Position Tracking.* When vehicles move on a bridge, the estimation of vehicle loads, vehicle positions, and structural parameters for bridges can be achieved with the method presented in Sections 3.3 and 3.4. However, when a vehicle is not on the bridge, e.g., the vehicle has not entered the bridge or the vehicle has exited the bridge, the corresponding location vector of vehicle load $\mathbf{L}_b(x)$ will stay at zero, implying that the vehicle loads will have no influence on the bridge responses. In this scenario, there will be infinite combinations of vehicle loads and vehicle positions that can satisfy both the state space equation and the observation equation.

Therefore, additional constraints on vehicle loads or vehicle positions are needed for the estimation.

Introduce a small positive number $x_{\text{entry}}$, e.g., $x_{\text{entry}} = 1\,\text{m}$. When a vehicle, say the $k$-th vehicle, is not on the bridge, set $x^{(k)}(t) = x_{\text{entry}}$, implying that the vehicle is waiting at the entrance of the bridge. Then, equation (3) can be rewritten as follows:

$$\mathbf{L}_b\left(x^{(k)}\right) = \begin{cases} \mathbf{L}_{b0}\left(x^{(k)}\right), & \text{when } 0 < x^{(k)} \le l_{\text{bridge}}, \\ \mathbf{L}_{b0}\left(x_{\text{entry}}\right), & \text{when } x^{(k)} \le 0 \text{ or } x^{(k)} > l_{\text{bridge}}, \end{cases} \quad (k = 1, 2, \ldots, N_v). \tag{23}$$

With this constraint, $\mathbf{L}_b(x^{(k)})$ is no longer a zero vector and the estimation of vehicle load can be conducted for the case where the vehicle is not on the bridge.

Based on the aforementioned rule, the specific constraint conditions are listed as follows:

(1) As mentioned at the end of Section 3.1, when the $k$-th vehicle exits the bridge, the corresponding elements, $x^{(k)}(t)$, $v^{(k)}(t)$, and $F^{(k)}(t)$, will be reset for the estimation of next vehicle.

(2) When the $k$-th vehicle is not on the bridge, set the estimated vehicle position $x^{(k)}(t) = x_{\text{entry}}$. Then,

(i) If there is no new vehicle, the estimated vehicle weight will stay at zero spontaneously.

(ii) If a new vehicle enters the bridge, the estimated vehicle weight will increase automatically. If the estimated vehicle weight $G^{(k)}(t)$ is larger than the threshold $G_{\text{thd}}$, which represents the entry of a new vehicle, the constraint on the estimated position will be removed and the estimation will continue with the EKF presented in Sections 3.3 and 3.4. In this study, $G_{\text{thd}}$ is taken as 5 kN.

(3) For the stability of the estimation, when the $k$-th vehicle is not on the bridge, reset the parameters regarding $P^{(k)}(t)$, i.e., $\mathbf{y}_f^{(k)}(t)$, $\boldsymbol{\theta}_f^{(k)}(t)$, and $\boldsymbol{\psi}_{\mathbf{w}}^{(k)}(t)$.

## 4. Summary of the Proposed Method

The implementation of the proposed method for the real-time simultaneous estimation of vehicle loads, vehicle positions, and structural parameters is summarized as follows:

**Initialization**:

Set initial values for $\mathbf{V}_{0|0}$, $\boldsymbol{\psi}_{0|0}$, $\boldsymbol{\Sigma}_{\mathbf{V},0|0}$, and $\boldsymbol{\Sigma}_{\boldsymbol{\psi},0|0}$.

**Recursive stage**:

**for** $i = 0$: $N$ **do**

(1) Compute the predicted state vector $\mathbf{V}_{i+1|i}$ and its covariance matrix $\boldsymbol{\Sigma}_{\mathbf{V},i+1|i}$ using equations (13) and (14), respectively.

(2) Compute the updated noise parameter vector $\boldsymbol{\psi}_{i+1|i+1}$ and its covariance matrix $\boldsymbol{\Sigma}_{\boldsymbol{\psi},i+1|i+1}$ using equations (21) and (22), respectively.

(3) Compute the updated state vector $\mathbf{V}_{i+1|i+1}$ and its covariance matrix $\boldsymbol{\Sigma}_{\mathbf{V},i+1|i+1}$ by EKF using equations (15)–(17).

(4) Supplementary constraints when a vehicle is not on the bridge:

**if** $x_{i+1|i+1}^{(k)} > l_{\text{bridge}}$ $(k = 1, 2, \cdots, N_v)$, **then**

Set $x_{i+1|i+1}^{(k)} = x_{\text{entry}}$, $v_{i+1|i+1}^{(k)} = 0$, $G_{i+1|i+1}^{(k)} = 0$

**end if**

**if** $G_{i+1|i+1}^{(k)} < G_{\text{thd}}$ $(k = 1, 2, \cdots, N_v)$, **then**

Set $x_{i+1|i+1}^{(k)} = x_{\text{entry}}$.

**end if**

**if** $x_{i+1|i+1}^{(k)} = x_{\text{entry}}$ $(k = 1, 2, \cdots, N_v)$, **then**

Set $\mathbf{y}_{f,i+1|i+1}^{(k)} = 0$, $\boldsymbol{\theta}_{f,i+1|i+1}^{(k)} = \boldsymbol{\theta}_{f,0|0}^{(k)}$, $\boldsymbol{\psi}_{\mathbf{w},i+1|i+1}^{(k)} = \boldsymbol{\psi}_{0|0}^{(k)}$

**end if**

**end for**

## 5. Illustrative Examples

Two illustrative examples are presented in this section to demonstrate the feasibility of the proposed method for vehicle load estimation, vehicle position tracking, and structural identification of a single-span or multispan bridges subjected to successive vehicle loads, including successive single/multiple vehicles with different weights and uniform/variable speeds.

*5.1. Example 1: Single-Span Bridge with Degrading Stiffness Subjected to Successive Vehicle Loads.* A single-span bridge shown in Figure 2 is considered in the first example. The span of the bridge structure is $S_{\text{bridge}} = 40\,\text{m}$. The bending stiffness and the mass per unit length of the bridge structure are $\text{EI} = 8.62 \times 10^9\,\text{N} \cdot \text{m}^2$ and $\rho A = 7.50 \times 10^3\,\text{kg/m}$, respectively. The bridge structure is modelled with 10 quadratic quadrilateral elements and the elements are divided into three groups as shown in Figure 2. The stiffness matrix is then characterized as $\mathbf{K} = \sum_{k=1}^{3} \theta_{\mathbf{K}}^{(k)} \mathbf{K}_{\text{sub}}^{(k)}$, where $\mathbf{K}_{\text{sub}}^{(k)}$ are the nominal stiffness submatrices and $\theta_{\mathbf{K}}^{(k)}$ are the stiffness parameters corresponding to each group of elements, respectively. The stiffness parameters are taken as $\theta_{\mathbf{K}}^{(k)} = 1$ for

the original undamaged structure. The first three natural frequencies of the bridge structure are 1.05, 4.20, and 9.41 Hz. The Rayleigh model $\mathbf{C} = \theta_{\mathbf{C}}^{(1)}\mathbf{M} + \theta_{\mathbf{C}}^{(2)}\mathbf{K}$ is adopted for the damping matrix with $\theta_{\mathbf{C}}^{(1)} = 0.2116\,\mathrm{s}^{-1}$ and $\theta_{\mathbf{C}}^{(2)} = 0.0012\,\mathrm{s}$, so the damping ratios of the first two modes are 2%.

The flexural strains of the bridge structure are measured using the sensors installed at the red points of the bridge shown in Figure 2, and the number of observed DOF is $N_o = 6$. The monitoring duration is $T = 50\,\mathrm{s}$ with the sampling time step taken as $t = 1/400\,\mathrm{s}$. It should be mentioned that for the illustrate example in this study, the strain measurements are simulated through the vehicle-bridge interaction dynamics introduced in Section 2. In addition, to consider the influences of measurement noises, 5% root mean square (RMS) noises are superimposed onto the time histories of strain measurements, i.e., the measurement noises are taken to be 5% root mean square (RMS) of the measured responses at midspan of the bridge. The covariance matrix of the measurement noises can be written as $\boldsymbol{\Sigma}_{\mathbf{n},i}(\psi_{\mathbf{n},i}) = (\sigma_{\mathbf{n}}^0)^2\mathbf{I}_{N_o}$. The initial augmented vector $\mathbf{V}_{0|0} = [\mathbf{y}_{f,0|0}^T, \mathbf{Y}_{b,0|0}^T, \dot{\mathbf{Y}}_{b,0|0}^T, \mathbf{x}_{0|0}^T, \mathbf{v}_{0|0}^T, \mathbf{G}_{0|0}^T, \quad \boldsymbol{\theta}_{f,0|0}^T, \boldsymbol{\theta}_{\mathbf{K},0|0}^T, \boldsymbol{\theta}_{\mathbf{C},0|0}^T]^T$ for estimation is taken as follows: $\mathbf{y}_{f,0|0}$, $\mathbf{Y}_{b,0|0}$, and $\dot{\mathbf{Y}}_{b,0|0}$ are taken as zero vectors; $\mathbf{x}_{0|0}$ and $\mathbf{v}_{0|0}$ are, respectively, taken as $x_{\mathrm{entry}}\mathbf{1}_{N_v\times 1}$ and zero; $\mathbf{G}_{0|0}$ is taken as zero; $\boldsymbol{\theta}_{\mathbf{K},0|0}$ and $\boldsymbol{\theta}_{\mathbf{C},0|0}$ are taken as 1.2 times of the actual values; and $\boldsymbol{\theta}_{f,0|0}$ is taken as $[10,1]^T$. The initial noise parameter vector is selected as $\psi_{0|0} = [\psi_{\mathbf{w},0|0}^T, \psi_{\mathbf{n},0|0}^T]^T = [1,\ 10\sigma_{\mathbf{n}}^0]^T$. These selections of initial values will be used throughout this example. The fading factors in equations (14) and (19) are taken to be $\lambda_1 = 2^{2/100}$, $\lambda_2 = 2^{2/500}$, $\lambda_3 = 2^{2/2000}$, and $\lambda_4 = 2^{2/2000}$ in this study, so the half-life of the past data for the estimation of vehicle positions, vehicle weights, structural parameters, and noise parameters is 100, 500, 2000, and 2000, respectively.

The vehicle-bridge coupled system is subjected to the excitation of road roughness and vehicle loads. The road roughness is modelled as a zero-mean homogeneous Gaussian random field with the power spectral density as follows [47]:

$$S(\omega) = \frac{4\gamma_1\gamma_2\gamma_3\omega_0^2}{\pi\left[\left(\omega_0^2 - \omega^2\right)^2 + 4\gamma_2^2\omega^2\right]}, \tag{24}$$

where $\gamma_1 = 5\times 10^{-6}\,\mathrm{m}^3\cdot\mathrm{rad}^{-1}$, $\gamma_2 = 0.5\,\mathrm{rad}\cdot\mathrm{m}^{-1}$, $\gamma_3 = 1.5\,\mathrm{rad}\cdot\mathrm{m}^{-1}$, and $\omega_0^2 = 2.5\,\mathrm{rad}^2\cdot\mathrm{m}^{-2}$. By using the spectral representation method [48], the sample of the road roughness is generated as shown in Figure 3.

In the following sections, several cases, including single or multiple vehicles with constant or variable speeds, are considered to investigate the feasibility of the proposed method. Additionally, the influence of the sensor layout is also discussed.

*5.1.1. Case 1: Successive Single Vehicles with Different Weights and Uniform Speeds.* Vehicles with uniform speed are considered in the first case and the corresponding vehicle positions, vehicle speeds, and vehicle weights are shown in Figures 4–6, respectively. During the monitoring duration, a total number of 16 vehicles pass across the bridge sequentially, where the passage of a single vehicle is represented by a triangle in Figure 4. The time intervals between the entries of two vehicles are taken as $t_{\mathrm{int}} \sim U(2.5\,\mathrm{s}, 3.5\,\mathrm{s})$ for considering randomness and the requirement of safety distance, where $U(\cdot)$ represents uniform distribution. To mimic the diversity of different vehicles, the vehicle speeds and vehicle weights are taken as $v = \phi_v$ and $G = \phi_G G_0$, respectively, where $\phi_v \sim \mathrm{U}(15\,\mathrm{m/s}, 25\,\mathrm{m/s})$ and $\phi_G \sim \mathrm{U}(0.5,1.5)$. Then, different vehicles have different speeds and different weights as shown in Figures 5 and 6. For each vehicle, the single-wheel vehicle model [47] shown in Figure 7 is adopted with the vehicle weight being $G = \phi_G G_0$, where $G_0 = (m_{v,0} + m_{w,0})g$ with $m_{v,0} = 5\times 10^3\,\mathrm{kg}$ and $m_{w,0} = 5\times 10^2\,\mathrm{kg}$ being the mass of the vehicle body and vehicle wheel, respectively. The stiffness and the damping of the suspension system of the vehicle are $k_{\mathrm{v},0} = 1.40\times 10^6\,\mathrm{N/m}$ and $c_{v,0} = 1.67\times 10^4\,\mathrm{N/(m/s)}$, respectively. The stiffness of the wheel is $k_{w,0} = 7.80\times 10^5\,\mathrm{N/m}$.

In addition, to further investigate the efficacy of the proposed method for structural identification, structural damages are imposed in this example. Sudden damage of 5% stiffness loss occurs at the left span of the bridge at $t = 30\,\mathrm{s}$ (i.e., $\theta_{\mathbf{K}}^{(1)}$ changes from 1 to 0.95).

Figures 8 and 9 show the estimated results of vehicle positions and vehicle speeds. The solid lines represent the actual values of vehicle positions and vehicle speeds, and the dashed lines represent the estimated results. The dashed lines correspond to the estimated results plus or minus three standard deviations, which implies the boundaries of the 99.7% credibility intervals of the estimation. The same line style will be used hereafter for other figures. Good agreements can be seen between the estimated results and the actual values, indicating that the proposed method can track the vehicle positions well for the case with uniform-speed vehicles. Figures 10 and 11 show the estimated results of vehicle loads and vehicle weights. For clarity, the estimation of the 8th vehicle is magnified and further shown in Figure 12. After the first few seconds, the estimated vehicle loads match the actual values well and the vehicle weights can be identified accurately, indicating the effectiveness of the filtered noise model for vehicle load estimation.

Figure 13 shows the estimation of structural parameters. After the severe fluctuation in the early estimation stage due to the poor initial values, the estimated structural parameters converge to the actual value. Additionally, the sudden damage of the structure at $t = 30\,\mathrm{s}$ can be well identified with negligible time-delay. Figure 14 shows the estimation of noise parameter and the result converges to a satisfactory value.

For comparison, the estimation is also conducted using the EKF scheme based on the random walk vehicle load model [24, 25]. Note that these schemes do not consider the position tracking of vehicles. Therefore, the estimation of vehicle loads and structural parameters for the bridge are conducted given vehicle positions. The augmented state vector for EKF in equation (10) is changed to $\mathbf{V}(t) = [\mathbf{Y}_b^T(t), \dot{\mathbf{Y}}_b^T(t), \mathbf{F}^T(t), \boldsymbol{\theta}_{\mathbf{K}}^T(t), \boldsymbol{\theta}_{\mathbf{C}}^T(t)]^T$, and the vehicle load vector is now given by the following equation:

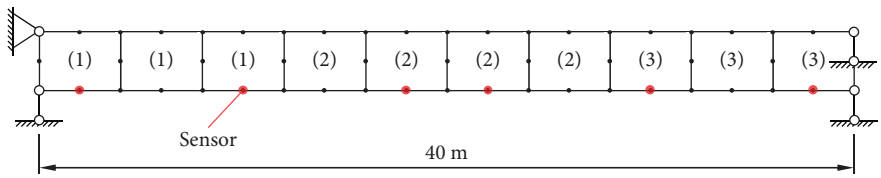


Figure 2: A single-span bridge.

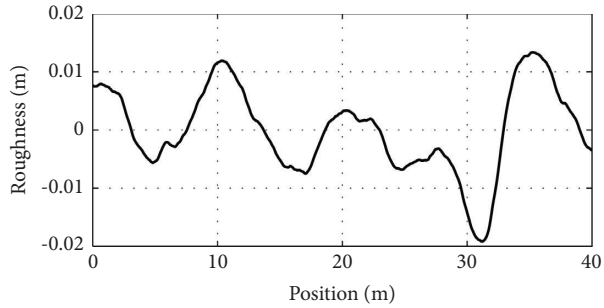


Figure 3: Road roughness.

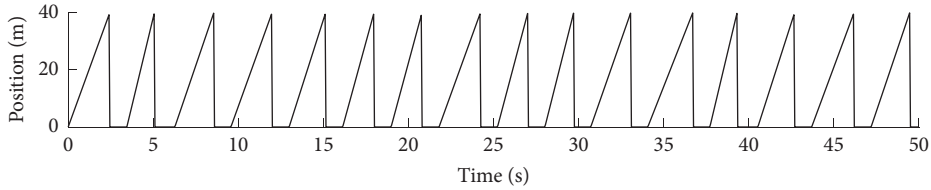


Figure 4: Time histories of vehicle positions.

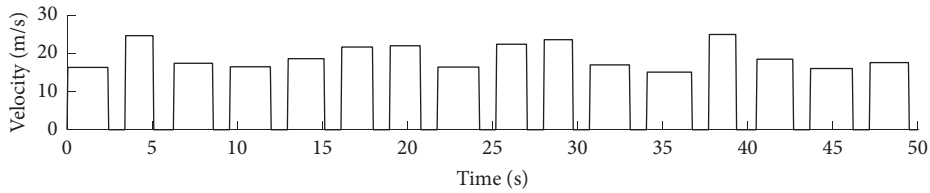


Figure 5: Time histories of vehicle speeds.

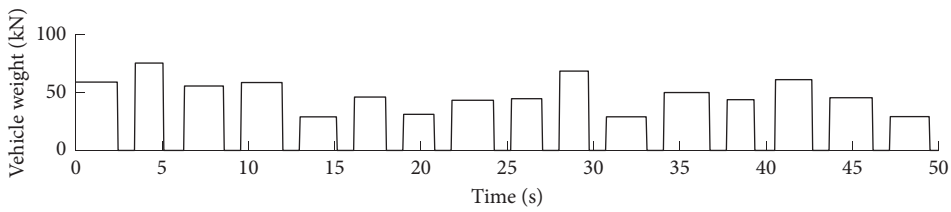


Figure 6: Time histories of vehicle weights.

$$\mathbf{F}_{i+1} = \mathbf{F}_i + \mathbf{w}_i, \tag{25}$$

where $\mathbf{w}_i = \mathbf{w}(t_i)$ is a zero-mean Gaussian random vector similar to that in equation (7).

Figure 15 shows the estimated results of vehicle loads. For clarity, the estimation for the 8th vehicle is also magnified and shown in Figure 16. One can compare Figure 16 with Figure 12(a); it can be found that the vehicle load estimation by the random walk model suffers from obvious time-delay in tracking while that by the proposed method does not suffer. Figure 17 shows the estimation of structural parameters. The identified results of the structural parameters are acceptable. In conclusion, the proposed method outperforms the random walk model in this case.

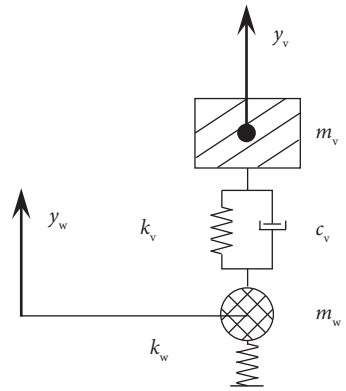


Figure 7: Single-wheel vehicle model.

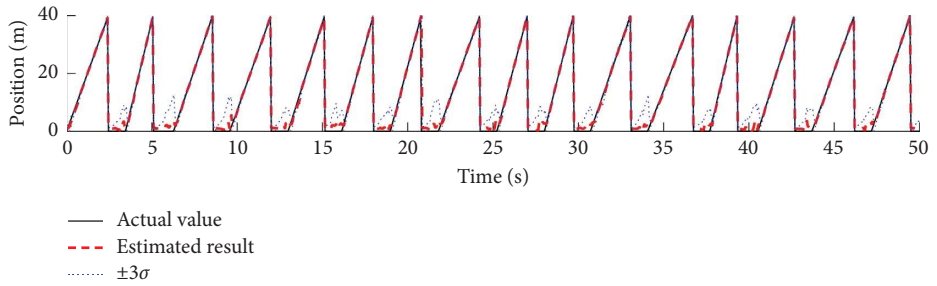


Figure 8: Estimated results of vehicle positions with the proposed method.

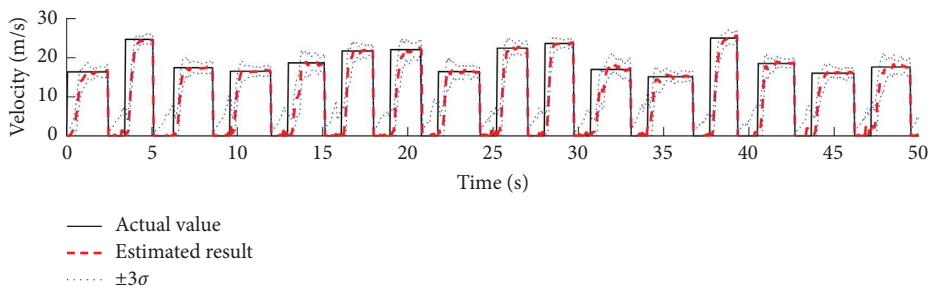


Figure 9: Estimated results of vehicle speeds with the proposed method.

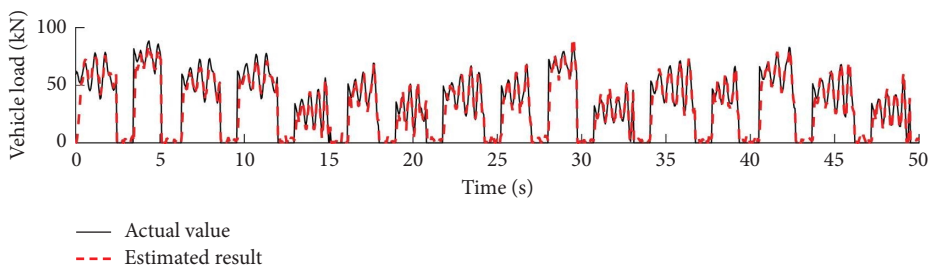


Figure 10: Estimated results of vehicle loads with the proposed method.

In addition to the estimation with filter technique in an online manner, vehicle load estimation and bridge structural identification are further conducted using the moving force identification (MFI) method [18] for comparison with the offline method. Figure 18 shows the estimated results of vehicle loads for the 8th vehicle using the method in [18]. By comparing Figure 18 with Figure 12(a), one can see that although some errors can still be seen at the beginning of the estimation, the overall estimation agrees well with the actual vehicle loads. In addition, the estimated structural parameter

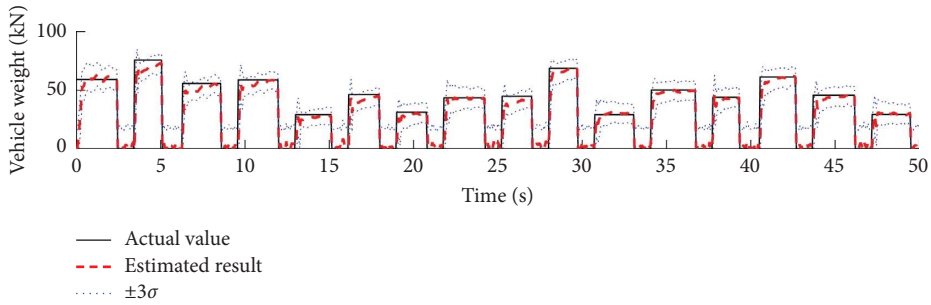


Figure 11: Estimated results of vehicle weights with the proposed method.

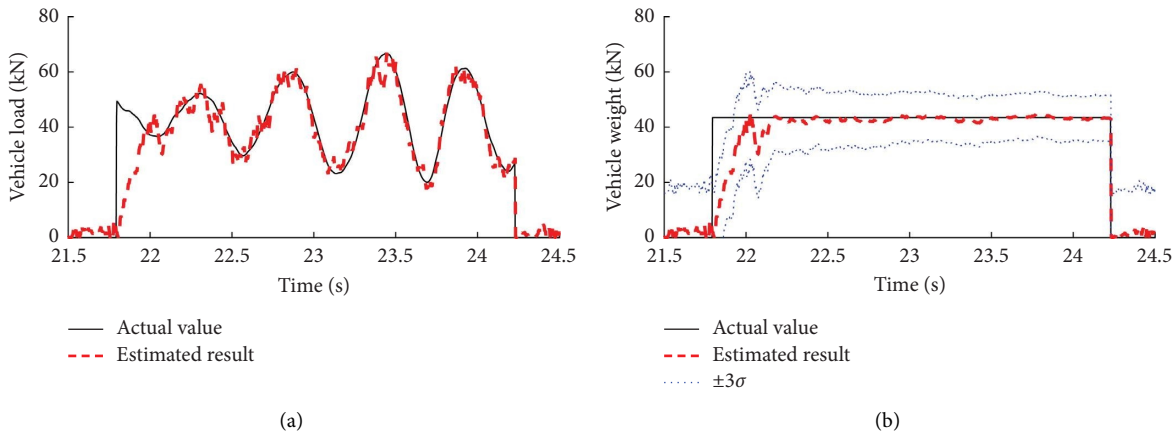


(a) (b)

Figure 12: Estimated results of vehicle load and vehicle weight for the 8th vehicle with the proposed method : (a) vehicle load and (b) vehicle weight.

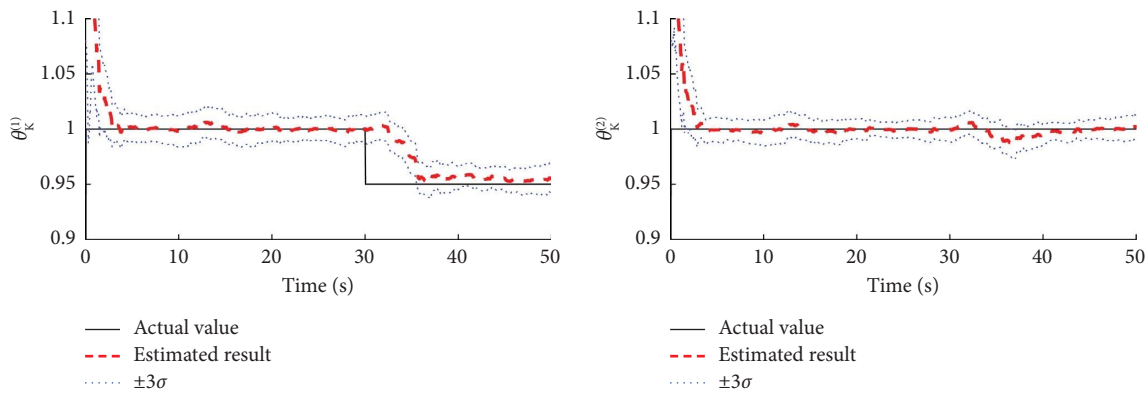


(a) (b)

Figure 13: Continued.

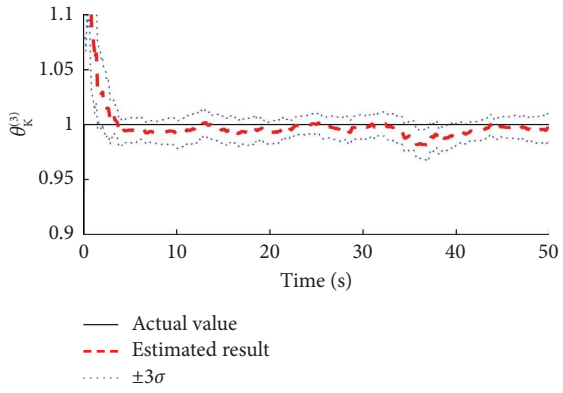


(c)

Figure 13: Estimated results of stiffness parameters with the proposed method: (a) stiffness parameter $\theta_K^{(1)}$, (b) stiffness parameter $\theta_K^{(2)}$, and (c) stiffness parameter $\theta_K^{(3)}$.

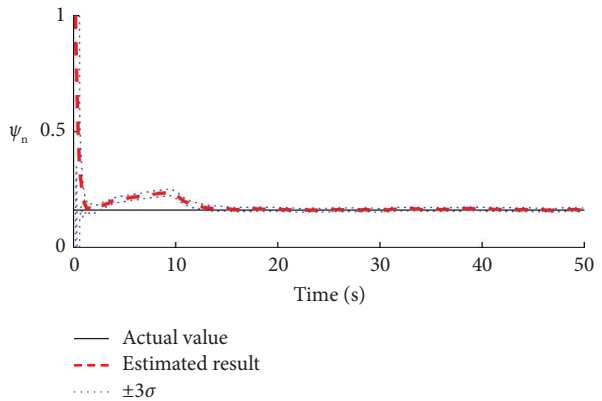


Figure 14: Estimated results of noise parameters with the proposed method.

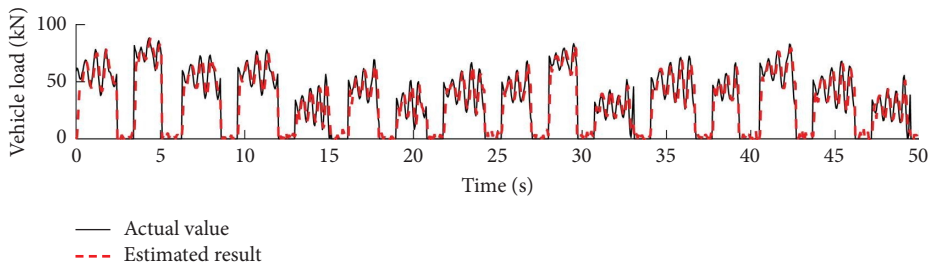


Figure 15: Estimated results of vehicle loads with the random walk model used in [24].

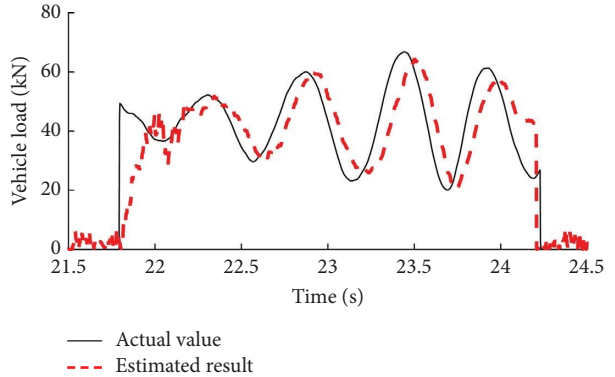


Figure 16: Estimated results of vehicle load for the 8th vehicle with the random walk model used in [24].

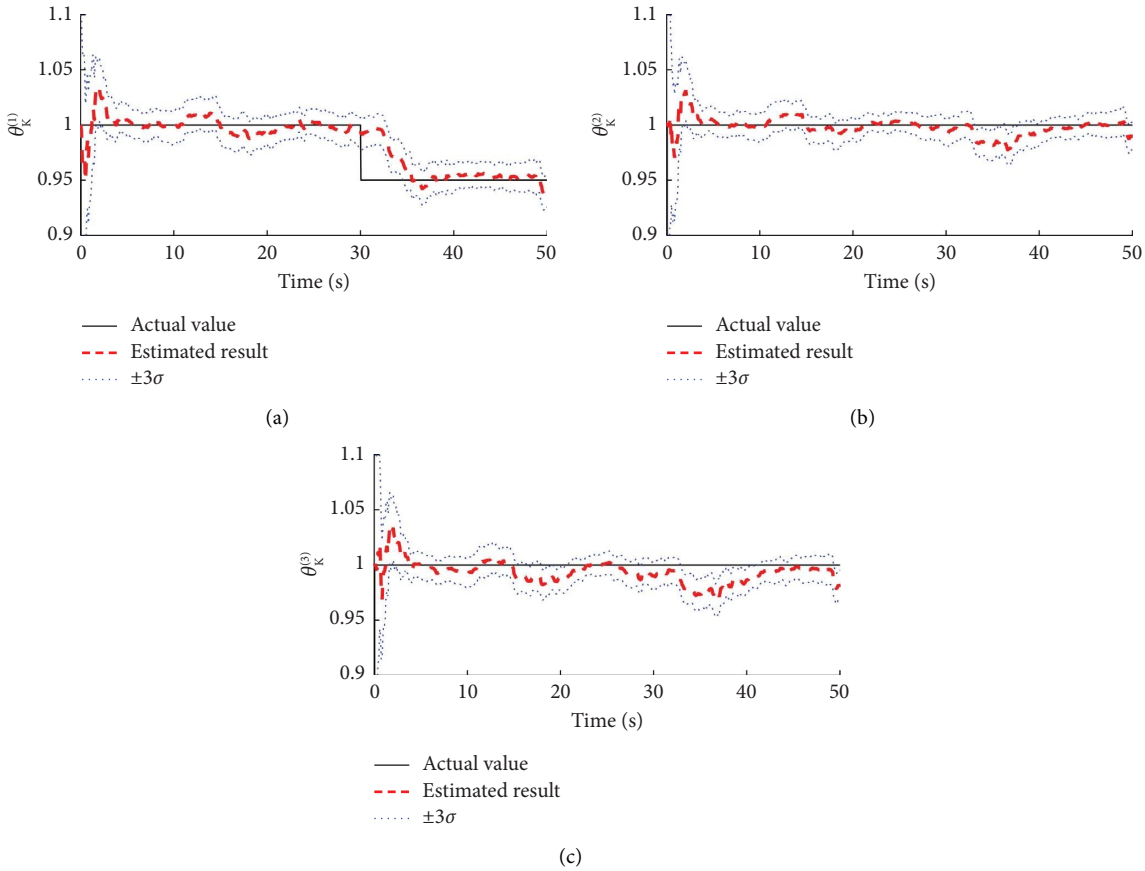


FIGURE 17: Estimated results of stiffness parameters with the random walk model used in [24]: (a) stiffness parameter $\theta_{\mathbf{K}}^{(1)}$, (b) stiffness parameter $\theta_{\mathbf{K}}^{(2)}$, and (c) stiffness parameter $\theta_{\mathbf{K}}^{(3)}$.

vector is $\boldsymbol{\theta}_{\mathbf{K}} = [0.996, 1.002, 1.003]^T$, which matches well with the actual values $\theta_{\mathbf{K}}^{(k)} = 1$ $(k = 1, 2, 3)$. However, it should be noted that the estimation using an offline manner can only estimate the average structural parameters in a certain time interval. When the damage occurs in the structure, e.g., $\theta_{\mathbf{K}}^{(1)}$ changes from 1 to 0.95 at $t = 30$ s, the variation of the structural parameters cannot be well identified, which may further affect the estimation of vehicle loads.

*5.1.2. Case 2: Successive Single Vehicles with Different Weights and Variable Speeds.* To further investigate the feasibility of the proposed method, the case where the vehicles moving with variable speeds is considered in this subsection, the corresponding vehicle positions, vehicle speeds, and vehicle loads are shown in Figures 19–21. Again, a total number of 16 vehicles pass across the bridge sequentially during the monitoring duration. The time intervals between vehicles, i.e., $t_{\text{int}}$, are same as those in Case 1.

To simulate the diversity of different vehicles, different speeds and different weights are taken for different vehicles as shown in Figures 20 and 21. For vehicle speeds, since vehicles usually accelerate when entering the bridge and decelerate when exiting the bridge, the time histories of the vehicle speeds shown in Figure 20 are assumed to be quadratic parabolas given by the following equation:

$$v(t) = \frac{3}{2\phi_{v2} + 1}\left[\phi_{v2}\phi_{v1} - (\phi_{v2} - 1)\phi_{v1}\left(\frac{2\phi_{v1}}{L_{\text{bridge}}}t - 1\right)^2\right], \tag{26}$$

where $\phi_{v1} \sim U(15\,\text{m/s}, 25\,\text{m/s})$ is the average speed and $\phi_{v2} \sim U(1.25,1.75)$ is the ratio of the maximum speed and minimum speed. For vehicle weights, $G = \phi_G G_0$ is used again with $\phi_G \sim U(0.5,1.5)$. However, an over-weight vehicle, the $10^{\text{th}}$ vehicle, occurs in this case with $G = 200$ kN as shown in Figure 21. Then, sudden damage of 5 % stiffness loss occurs at the left span of the bridge at $t = 30$ s (i.e., $\theta_{\mathbf{K}}^{(1)}$ changes from 1 to 0.95). The single-wheel vehicle model introduced in Case 1 is used again for each vehicle.

Figures 22 and 23 show the estimated results of vehicle positions and vehicle speeds. Similar to the results in Case 1, good agreements can be seen between the estimated results and the actual values. The acceleration and deceleration of vehicles are well identified, indicating that with the time-varying speed vector $\mathbf{v}(t)$ adopted in equation (10), the proposed method can also track the vehicle positions well even for the vehicles with variable speeds. Figures 24 and 25 show the estimated results of vehicle loads and vehicle weights. Again, the estimation of the 8th vehicle is magnified and shown in Figure 26. After the first few seconds, the estimated vehicle loads and vehicle weights match the actual

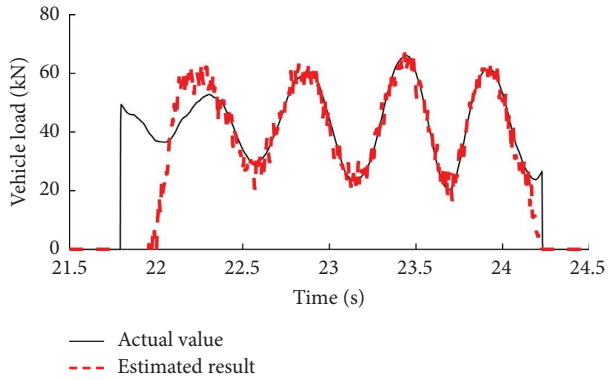


Figure 18: Estimated results of vehicle load for the 8th vehicle with the method in [18].

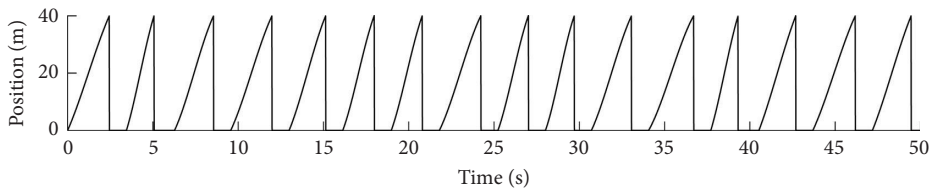


Figure 19: Time histories of vehicle positions.

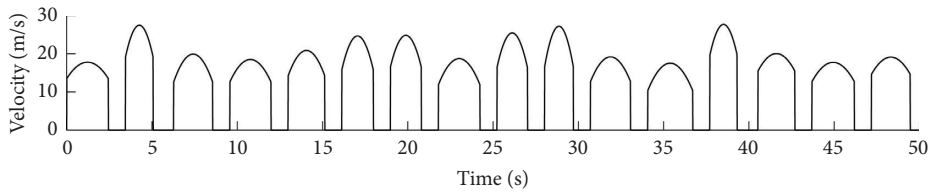


Figure 20: Time histories of vehicle speeds.

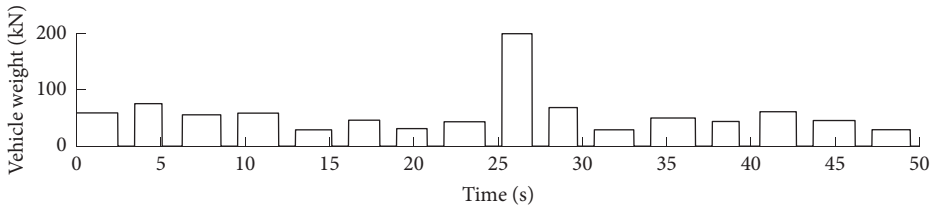


Figure 21: Time histories of vehicle weights.

values well. In addition, the sudden occurrence of the overweight vehicle at $t = 25$ s can also be identified accurately, showing the efficacy of the proposed method for vehicle load estimation.

Figure 27 shows the estimation of stiffness parameters. Again, the estimated structural parameters make a good agreement with the actual values, and the sudden reduction of the stiffness parameters at $t = 30$ s can be well captured with small time-delay. Figure 28 shows the estimation of noise parameter and the result is again satisfactory.

*5.1.3. Case 3: Successive Multiple Vehicles with Different Weights and Variable Speeds.* Successive multiple vehicles moving on the bridge are considered. The corresponding vehicle positions, vehicle speeds, and vehicle loads are shown in Figures 29–31. A total number of 23 vehicles pass across the bridge sequentially during the monitoring duration. The time intervals between vehicles are taken as $t_{\text{int}} \sim U(1.5\,\text{s}, 2.5\,\text{s})$. The parabolic-shape time histories of vehicle speeds shown in equation (26) are adopted again with $\phi_{v1} \sim U(12\,\text{m/s}, 15\,\text{m/s})$ and $\phi_{v2} \sim U(1.25,1.75)$. As the

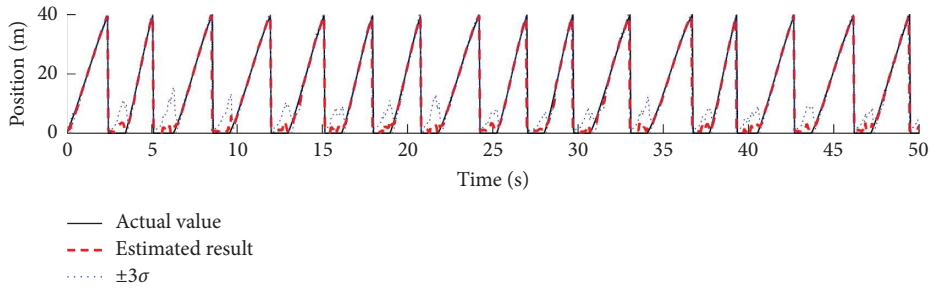


Figure 22: Estimated results of vehicle positions with the proposed method.

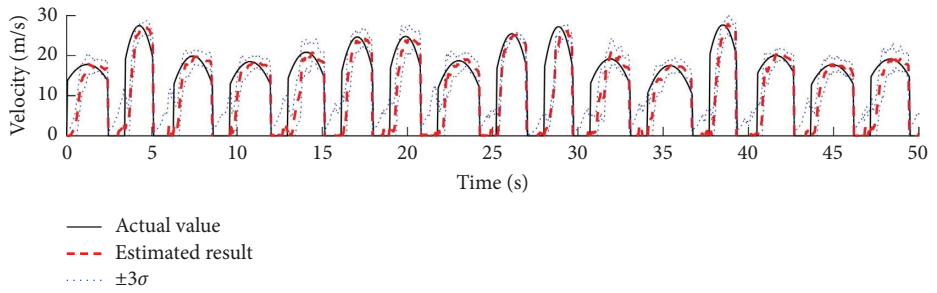


Figure 23: Estimated results of vehicle speeds with the proposed method.

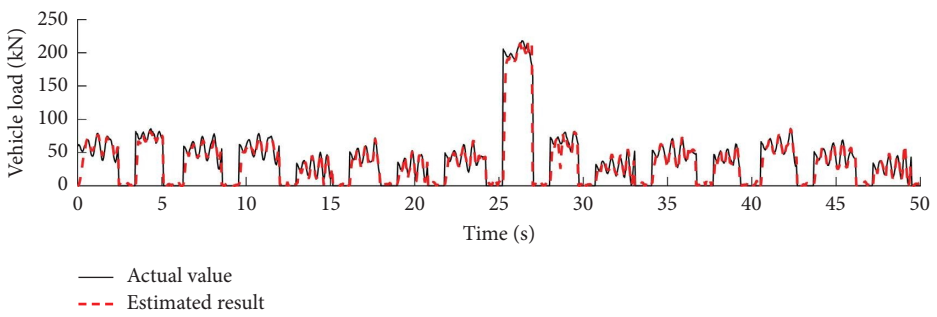


Figure 24: Estimated results of vehicle loads with the proposed method.

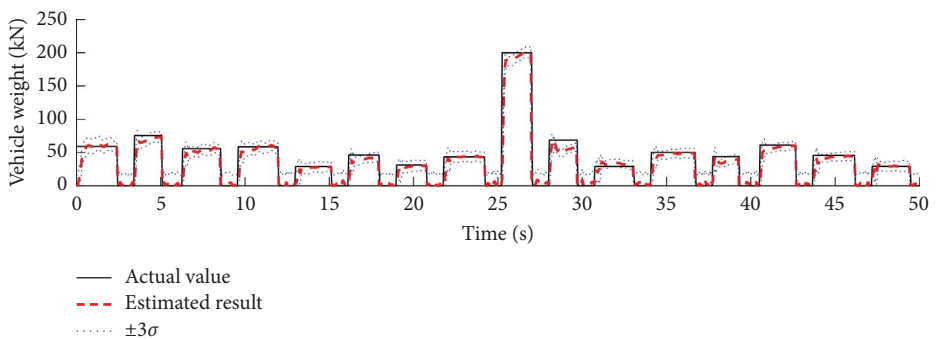


Figure 25: Estimated results of vehicle weights with the proposed method.

vehicle speeds become smaller in this case, two vehicles move on the bridge simultaneously as shown in Figure 29. The vehicle weights are taken as $G = \phi_G G_0$ with $\phi_G \sim U(0.5,1.5)$. The single-wheel vehicle model introduced in Case 1 is used for each vehicle. Additionally, sudden damage of 8 % stiffness loss at the left span of the bridge is imposed at $t = 30\,s$ (i.e., $\theta_{\mathbf{K}}^{(1)}$ changes from 1 to 0.92).

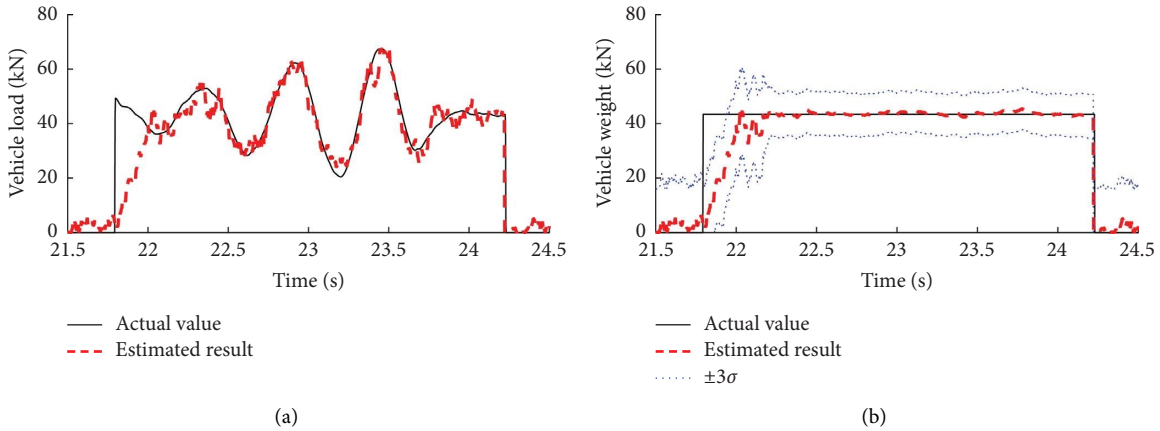


FIGURE 26: Estimated results of vehicle load and vehicle weight for the 8th vehicle with the proposed method: (a) vehicle load and (b) vehicle weight.

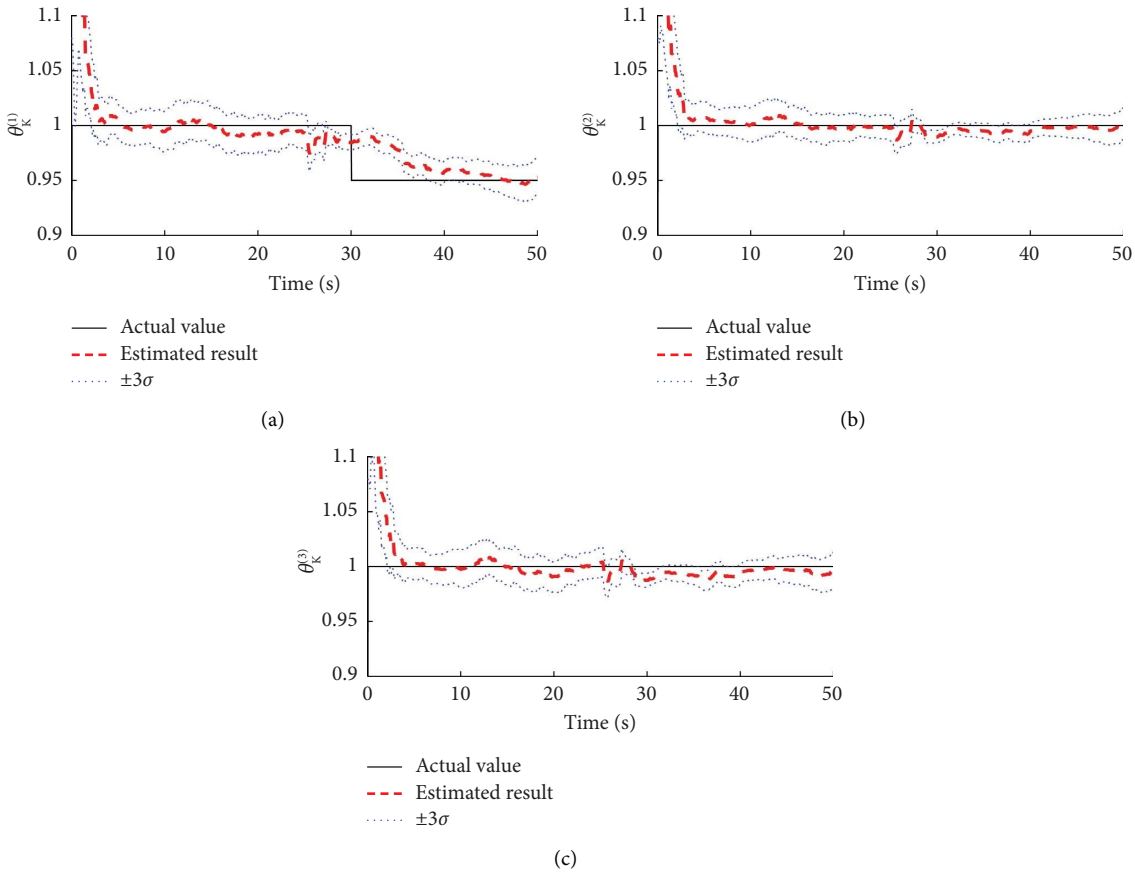


FIGURE 27: Estimated results of stiffness parameters with the proposed method: (a) stiffness parameter $\theta_{\mathbf{K}}^{(1)}$, (b) stiffness parameter $\theta_{\mathbf{K}}^{(2)}$, and (c) stiffness parameter $\theta_{\mathbf{K}}^{(3)}$.

Figures 32 and 33 show the estimated results of vehicle positions and vehicle speeds. For the case where multiple vehicles move on the bridge simultaneously, the positions of the vehicles are, respectively, estimated with the corresponding elements in $\mathbf{x}(t)$, and the results are presented in Figures 32(a) and 32(b). It can be seen that the estimated position agrees well with the actual values for each vehicle. Even though multiple vehicles affect the bridge responses simultaneously, the position tracking for each vehicle can still be well performed with the proposed methods. Analogously, Figures 34 and 35 show the estimated results of vehicle loads and vehicle weights. The magnified results for the 12$^{\text{th}}$ vehicle are presented in Figure 36. The vehicle load and vehicle weight for each vehicle are well distinguished

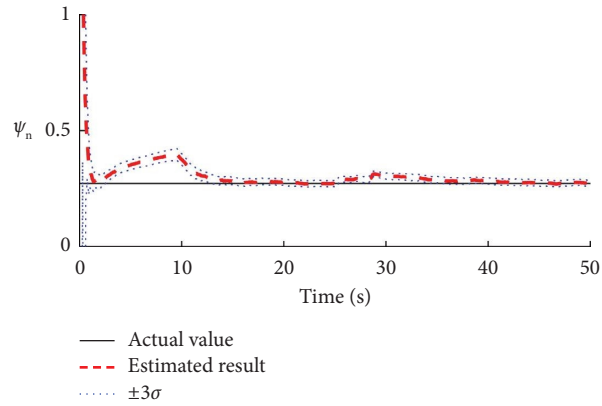


Figure 28: Estimated results of noise parameters with the proposed method.

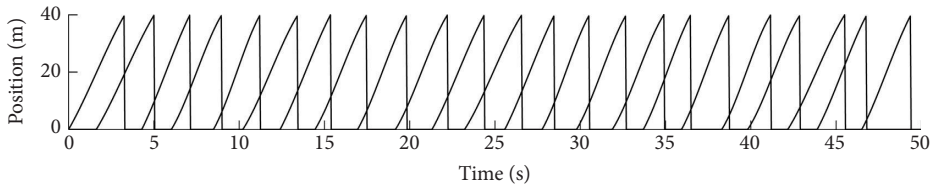


Figure 29: Time histories of vehicle positions.

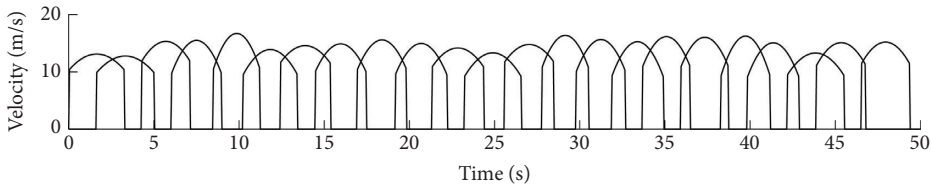


Figure 30: Time histories of vehicle speeds.

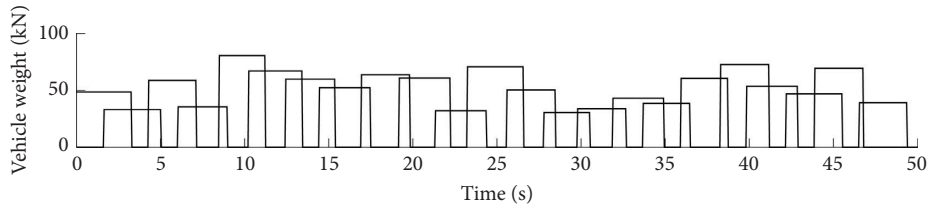


Figure 31: Time histories of vehicle weights.

and accurately estimated. Figure 37 shows the estimated stiffness parameters. The estimated results match well with the actual ones.

*5.1.4. Case 4: Investigation of Sensor Layout.* In this case, the influence of sensor layout is investigated. To distinct with the original layout of sensors shown in Figure 2 which evenly distributed along the bridge structure, the sensors are rearranged on one side of the bridge as shown in Figure 38. The flexural strains at the red points are measured and the number of measurements is still $N_o = 6$. The vehicle loads are the same as those in Case 1.

Figures 39 and 40 show the estimated results of vehicle positions and vehicle speeds. Figures 41 and 42 show the estimated results of vehicle loads and vehicle weights. Figure 43 shows the estimation of structural parameters. The estimated results of vehicle position, vehicle speeds, vehicle loads, and vehicle weights are basically the same as those obtained with evenly distributed sensors. However, obvious errors and large uncertainties can be seen in the estimated structural parameter of the third group of elements in Figure 43(c). This is because all the sensors are arranged merely on the left side of the bridge structure, and the information about the structural parameter of the third group

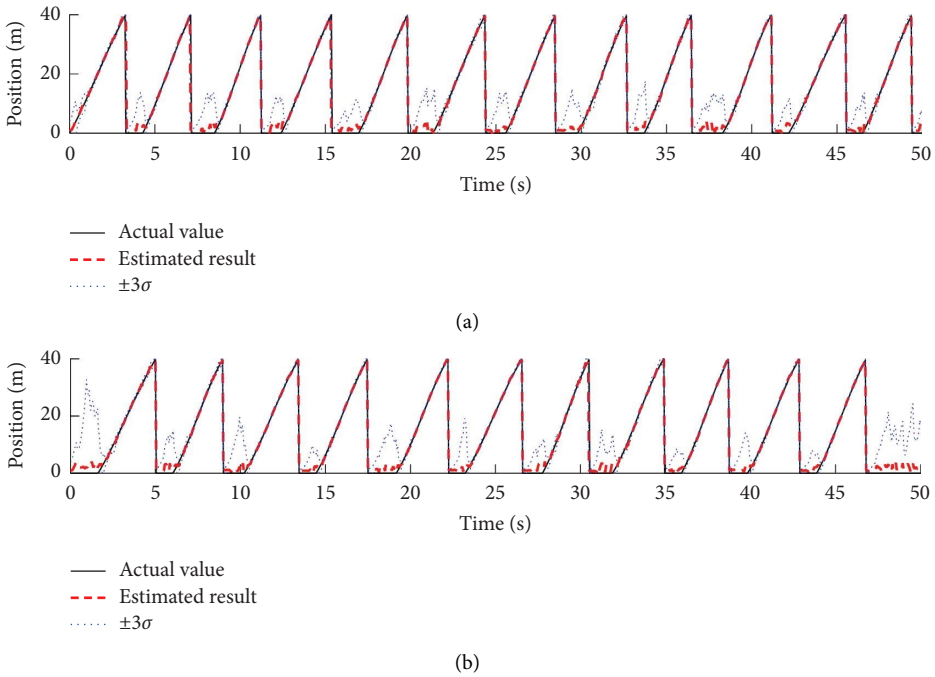


Figure 32: Estimated results of vehicle positions with the proposed method: (a) first group of vehicles and (b) second group of vehicles.

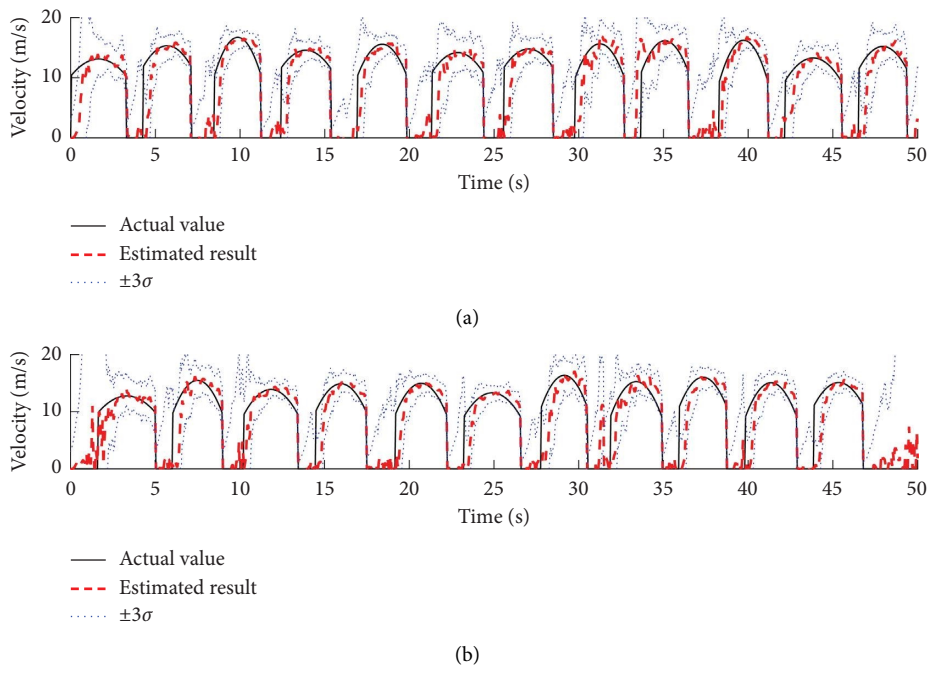


Figure 33: Estimated results of vehicle speeds with the proposed method: (a) first group of vehicles and (b) second group of vehicles.

of elements from measurements is not enough for the structural identification. Therefore, even arrangement of the sensors along the bridge structure is better for the estimation.

*5.2. Example 2: Multispan Continuous Bridge with Degrading Stiffness Subjected to Successive Vehicle Loads.* Successive multiple vehicles moving on a bridge are considered. Figure 44 shows a multispan continuous bridge structure. The

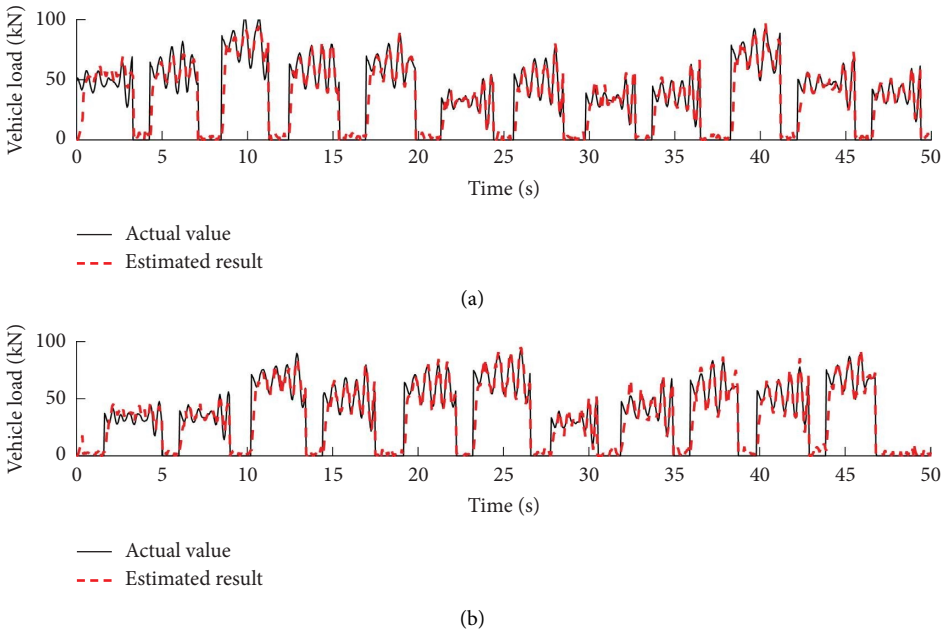


Figure 34: Estimated results of vehicle loads with the proposed method: (a) first group of vehicles and (b) second group of vehicles.

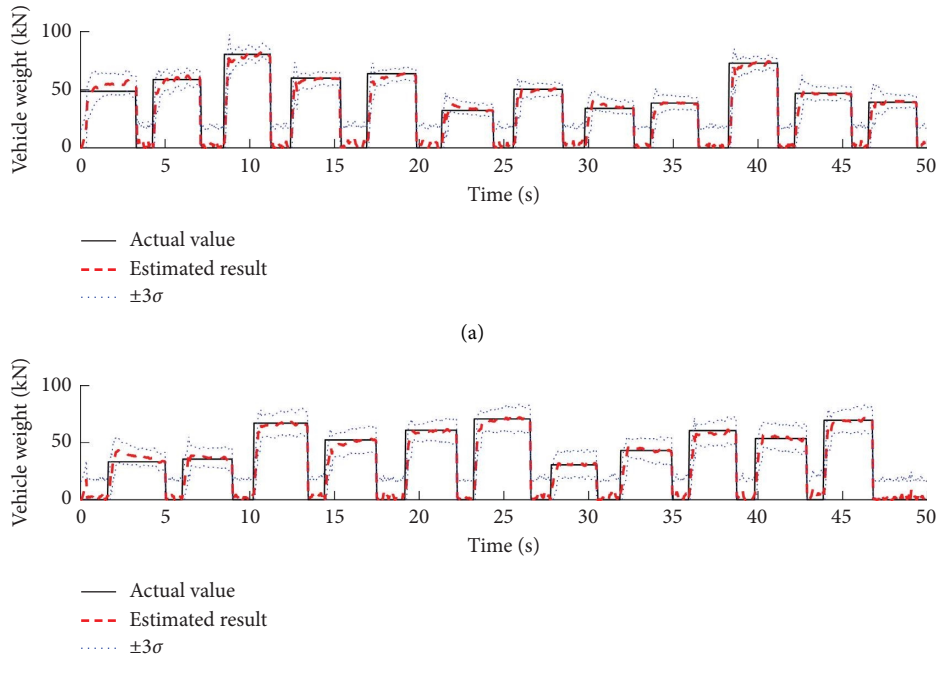


Figure 35: Estimated results of vehicle weights with the proposed method: (a) first group of vehicles and (b) second group of vehicles.

total length of the bridge is $l_{\text{bridge}} = 200$ m with each span being 50 m. The bending stiffness and the mass per unit length of the bridge structure are $\text{EI} = 8.63 \times 10^9\ \text{N} \cdot \text{m}^2$ and $\rho A = 7.50 \times 10^3$ kg/m, respectively. The bridge structure is modelled with 20 quadratic quadrilateral elements. The elements are divided into four parts, each with one stiffness parameter as shown in Figure 44, and thus the stiffness matrix is taken as $\mathbf{K} = \sum_{k=1}^{4} \theta_{\mathbf{K}}^{(k)} \mathbf{K}_{\text{sub}}^{(k)}$ with $\theta_{\mathbf{K}}^{(k)} = 1$ for the original structure. The first three natural frequencies are 0.68, 0.80, and 1.10 Hz. The Rayleigh model $\mathbf{C} = \theta_{\mathbf{C}}^{(1)} \mathbf{M} +$

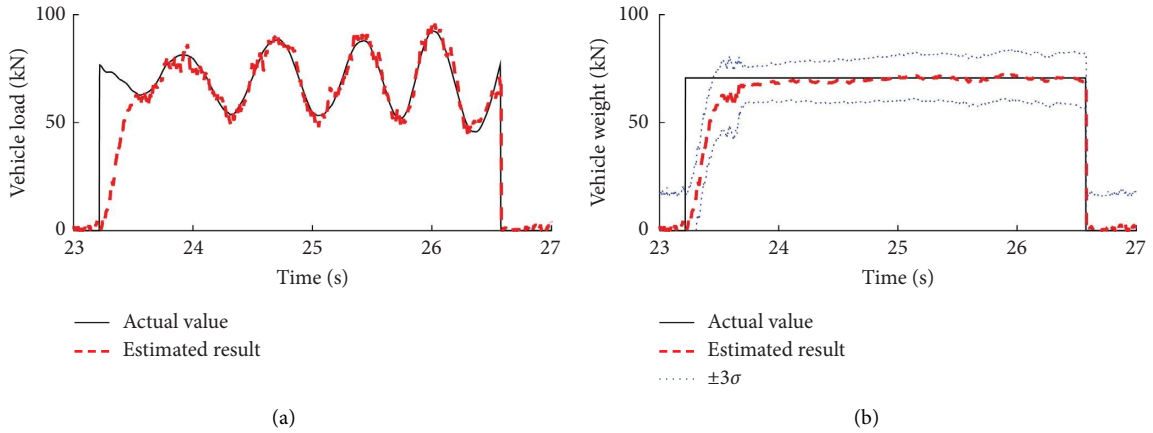


FIGURE 36: Estimated results of vehicle load and vehicle weight for the 8th vehicle with the proposed method: (a) vehicle load and (b) vehicle weight.

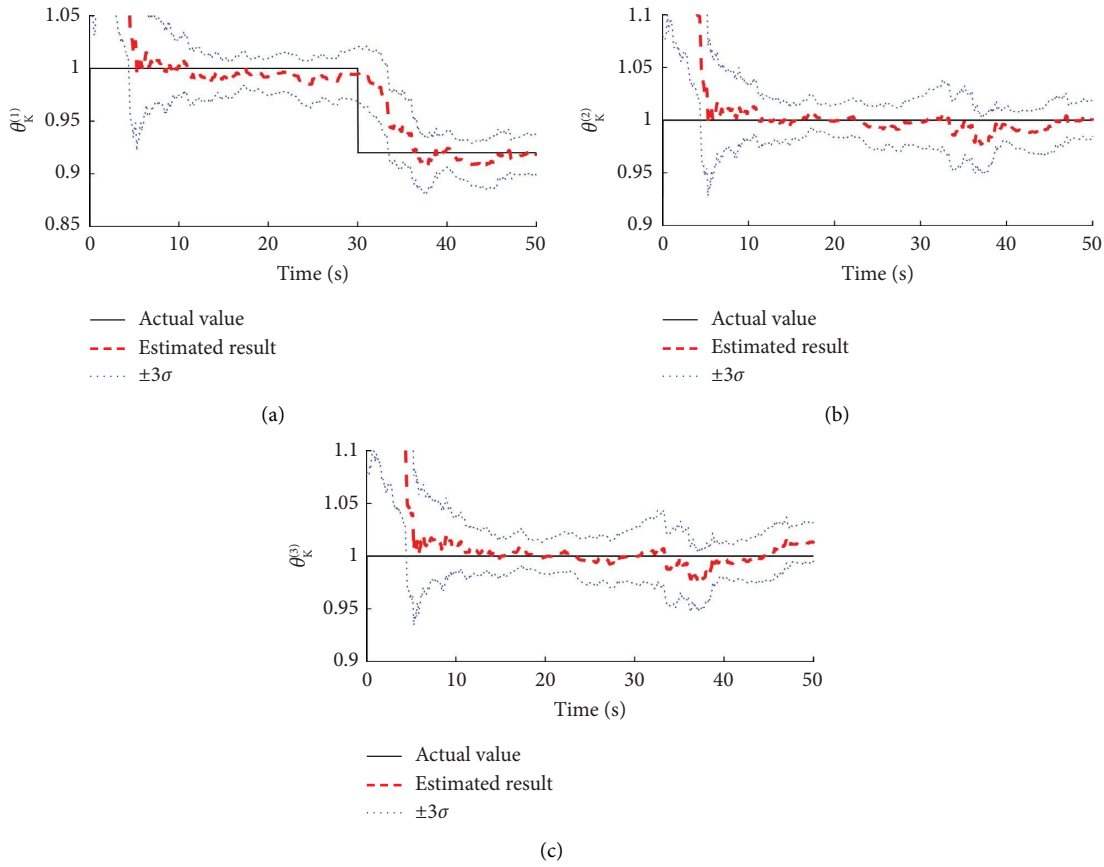


FIGURE 37: Estimated results of stiffness parameters with the proposed method: (a) stiffness parameter $\theta_{\mathbf{K}}^{(1)}$, (b) stiffness parameter $\theta_{\mathbf{K}}^{(2)}$, and (c) stiffness parameter $\theta_{\mathbf{K}}^{(3)}$.

$\theta_{\mathbf{C}}^{(2)}\mathbf{K}$ is adopted for the damping matrix with $\theta_{\mathbf{C}}^{(1)} = 0.1569\,\mathrm{s}^{-1}$ and $\theta_{\mathbf{C}}^{(2)} = 0.0008\,\mathrm{s}$, so the damping ratios of the first and the tenth modes are 2%.

The flexural strains at the red points marked in Figure 44 are measured for estimation and the number of observed DOF is $N_o = 8$. The monitoring duration is $T = 140\,\mathrm{s}$ with the sampling time step taken as $\Delta t = 1/400\,\mathrm{s}$. The measurement noises are taken to be 5% root mean square (RMS) of the measured responses at midspan of the bridge, and the covariance matrix of the measurement noise is then given by $\mathbf{\Sigma}_{\mathbf{n},i}(\psi_{\mathbf{n},i}) = (\sigma_{\mathbf{n}}^0)^2\mathbf{I}_{N_o}$. The initial values for the augmented vector $\mathbf{V}_{0|0}$ and the noise parameter vector $\psi_{0|0}$ are taken in the similar fashion as example 1. Structural damages are also imposed during the monitoring duration.

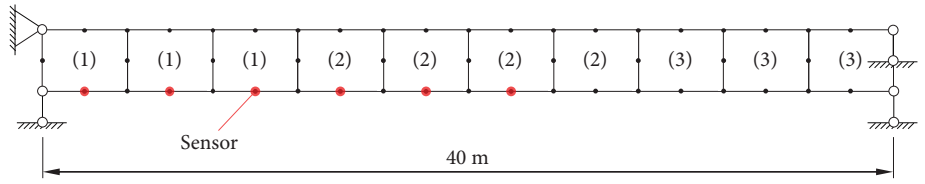


Figure 38: Layout of sensors.

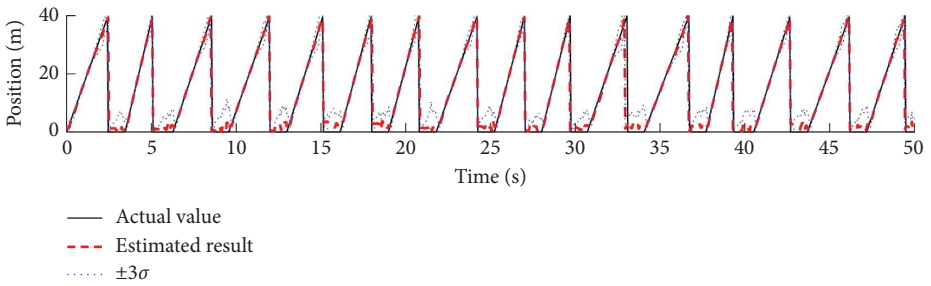


Figure 39: Estimated results of vehicle positions with the proposed method.

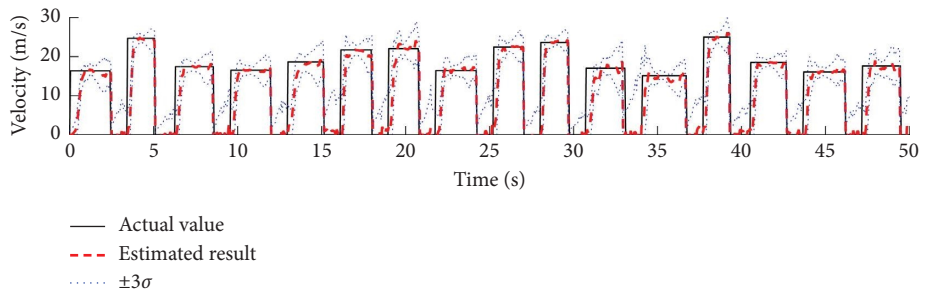


Figure 40: Estimated results of vehicle speeds with the proposed method.

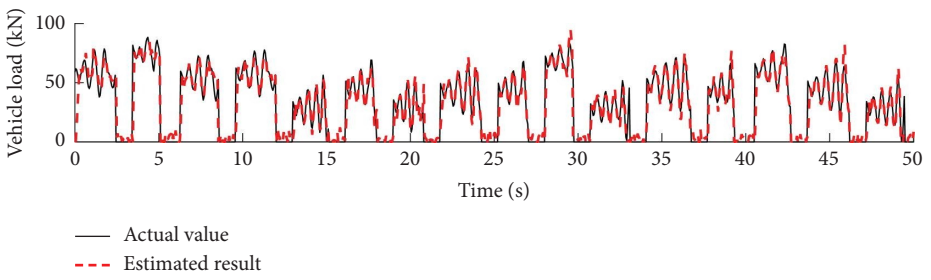


Figure 41: Estimated results of vehicle loads with the proposed method.

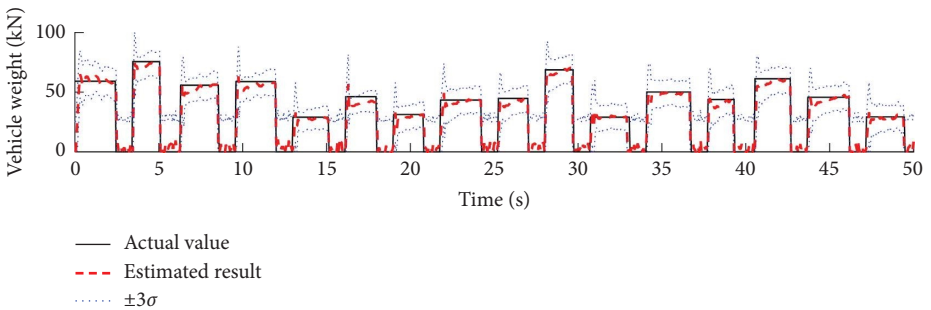


Figure 42: Estimated results of vehicle weights with the proposed method.

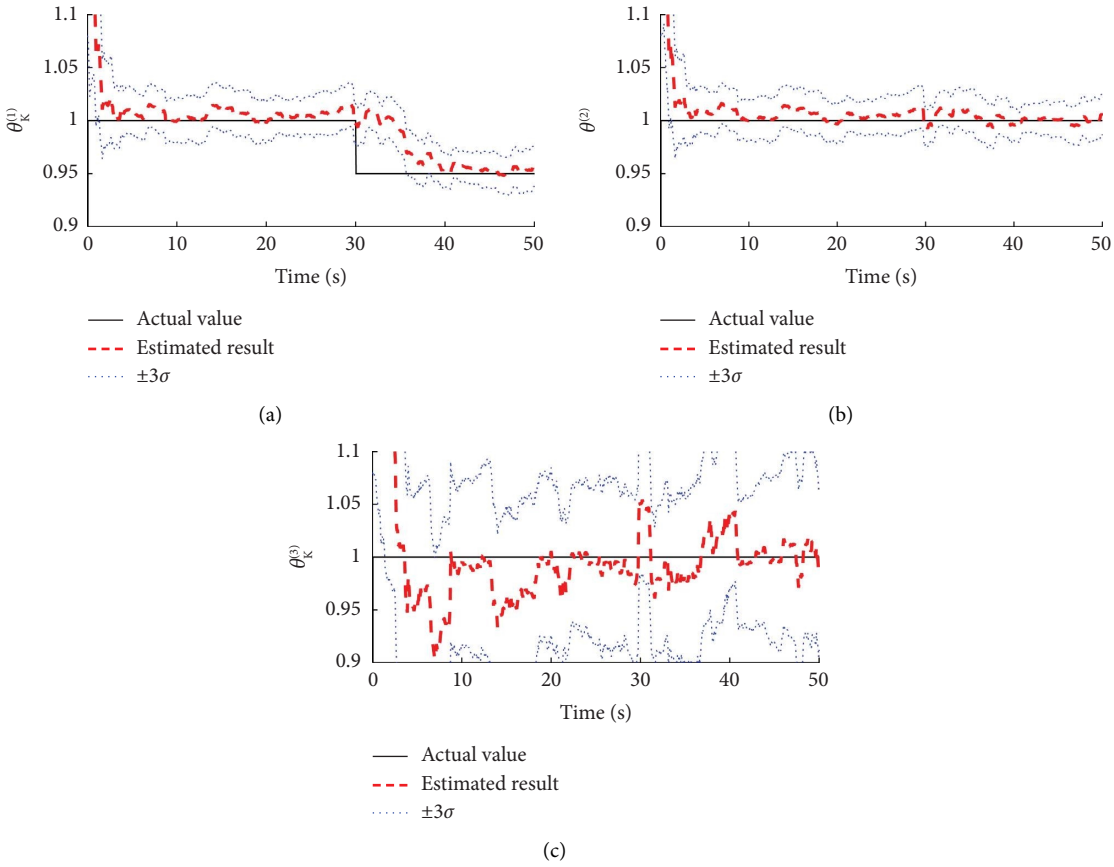


Figure 43: Estimated results of stiffness parameters with the proposed method: (a) stiffness parameter $\theta_{\mathbf{K}}^{(1)}$, (b) stiffness parameter $\theta_{\mathbf{K}}^{(2)}$, and (c) stiffness parameter $\theta_{\mathbf{K}}^{(3)}$.

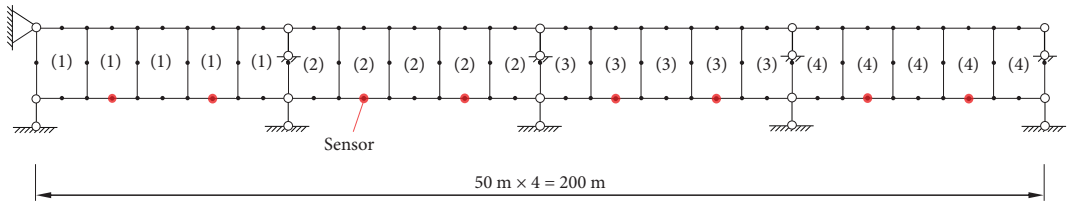


Figure 44: A multispan continuous bridge.

Sudden damage of 5% stiffness loss occurs at the left span of the bridge at $t = 80$ s (i.e., $\theta_{\mathbf{K}}^{(1)}$ changes from 1 to 0.95). Then, another sudden damage of 8% stiffness loss occurs at the midspan of the bridge at $t = 100$ s (i.e., $\theta_{\mathbf{K}}^{(3)}$ changes from 1 to 0.92).

The vehicle-bridge coupled system is subjected to the excitation of road roughness and vehicle loads. The road roughness model shown in equation (24) is used again with $\gamma_1 = 3 \times 10^{-5}\,\mathrm{m}^3 \cdot \mathrm{rad}^{-1}$, $\gamma_2 = 0.1\,\mathrm{rad} \cdot \mathrm{m}^{-1}$, $\gamma_3 = 0.3\,\mathrm{rad} \cdot \mathrm{m}^{-1}$, and $\omega_0^2 = 0.1\,\mathrm{rad}^2 \cdot \mathrm{m}^{-2}$, and the sample is presented in Figure 45. For vehicle loads, in order to investigate the influence of the axle configuration of vehicles on the vehicle load estimation, two kinds of vehicle models for the simulation of the vehicle-bridge coupled vibration are employed in the following section. One is the single-wheel vehicle model [47] adopted in Section 5.1.1, and the other is the two-axle vehicle model [18].

*5.2.1. Case 1: Simulation with Single-Wheel Vehicle Model.* As the bridge is long enough, multiple-vehicle passing case is investigated. The corresponding vehicle positions, vehicle speeds, and vehicle loads are shown in Figures 46–48. During the monitoring duration, a total number of 38 vehicles pass across the bridge sequentially with the time intervals between vehicles taken as $t_{\mathrm{int}} \sim U(3\,\mathrm{s}, 4\,\mathrm{s})$. Again, different speeds and different weights are taken for different vehicles as shown in Figures 47 and 48. For vehicle speeds, the parabolic-shape time histories of vehicle speeds shown in equation (26) are used with $\phi_{v1} \sim U(20\,\mathrm{m/s}, 25\,\mathrm{m/s})$ and $\phi_{v2} \sim U(1.25,1.75)$. For vehicle weights, the single-wheel vehicle model used in Section 5.1.1 is adopted with vehicle weights $G = \phi_G G_0$ and $\phi_G \sim U(0.5,1.5)$. In this example, the maximum number of the vehicles moving on the bridge simultaneously is $N_v = 3$.

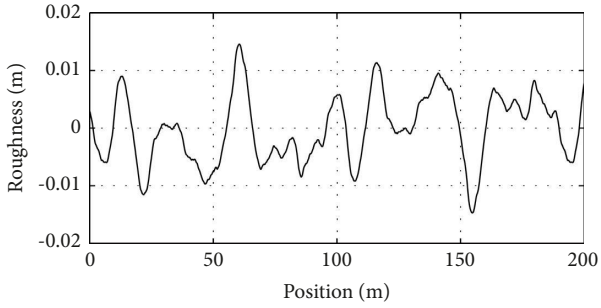


Figure 45: Road roughness.

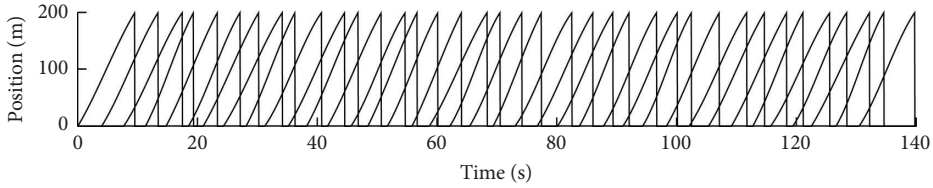


Figure 46: Time histories of vehicle positions.

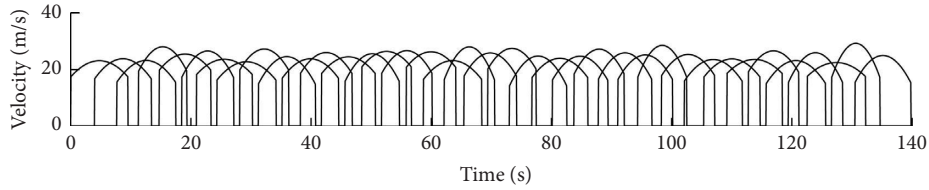


Figure 47: Time histories of vehicle speeds.

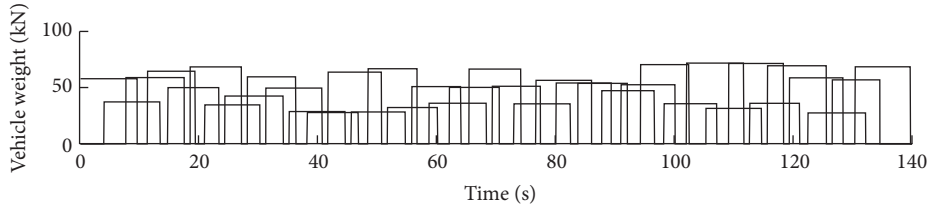


Figure 48: Time histories of vehicle weights.

Figures 49 and 50 compare the estimated results and actual values for vehicle positions and vehicle speeds. Good agreements can be seen indicating the efficacy of the proposed method for position tracking. Figures 51 and 52 show the estimated results of vehicle loads and vehicle weights. For clarity, the magnified results for the 13$^{th}$ vehicle are presented in Figure 53. After the first few seconds, the vehicle load and vehicle weight of the 13$^{th}$ vehicle are well estimated demonstrating that the proposed method can provide satisfactory results for vehicle load estimation. Figure 54 shows the estimated stiffness parameters. The estimated results match well with the actual ones, and the sudden decrease of $\theta_{\mathbf{K}}^{(1)}$ and $\theta_{\mathbf{K}}^{(3)}$ can be well identified.

*5.2.2. Case 2: Simulation with Two-Axle Vehicle Model.* The vehicle load estimation and bridge structural identification under the simulation with two-axle vehicle model are investigated in this section. The corresponding vehicle positions, vehicle speeds, and vehicle loads are shown in Figures 55–57. During the monitoring duration, a total number of 37 vehicles pass across the bridge sequentially. The random models for generating the time histories of vehicle positions and vehicle speeds are the same as those adopted in Section 5.2.1. For vehicle weights, the two-axle vehicle model [18] shown in Figure 58 is adopted. The axle spacing is $a = 4.27$ m with $a_1 = 2.42$ m and $a_2 = 1.85$ m. The mass and the moment of inertia of the vehicle body are

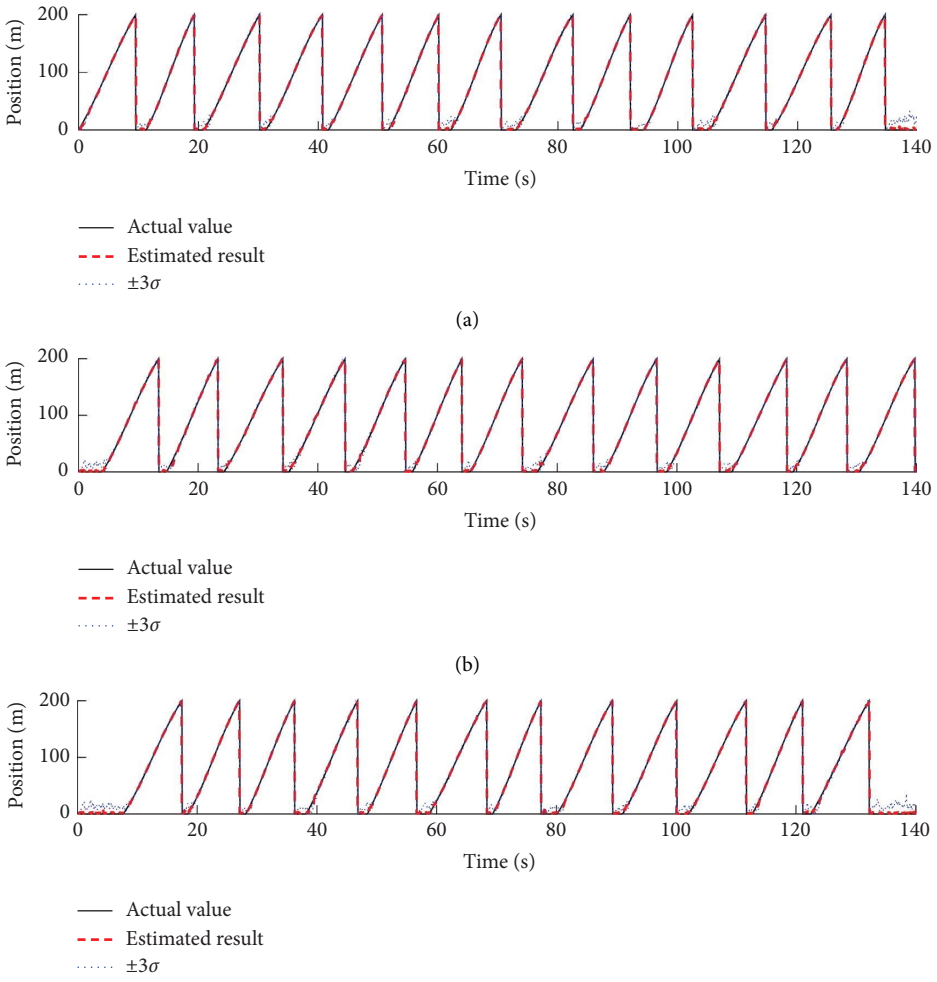


Figure 49: Estimated results of vehicle positions with the proposed method: (a) first group of vehicles, (b) second group of vehicles, and (c) third group of vehicles.

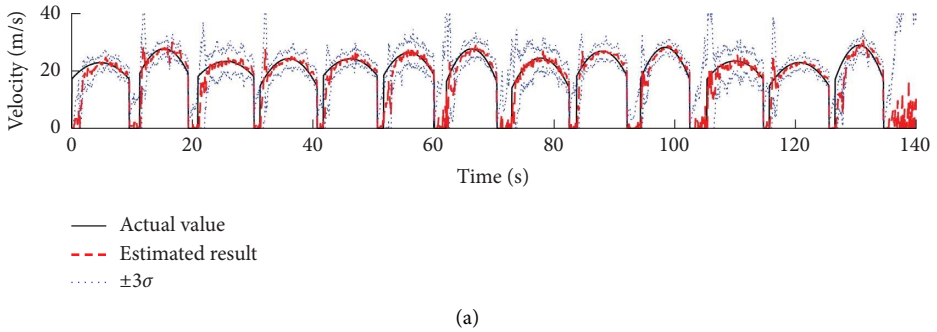


Figure 50: Continued.

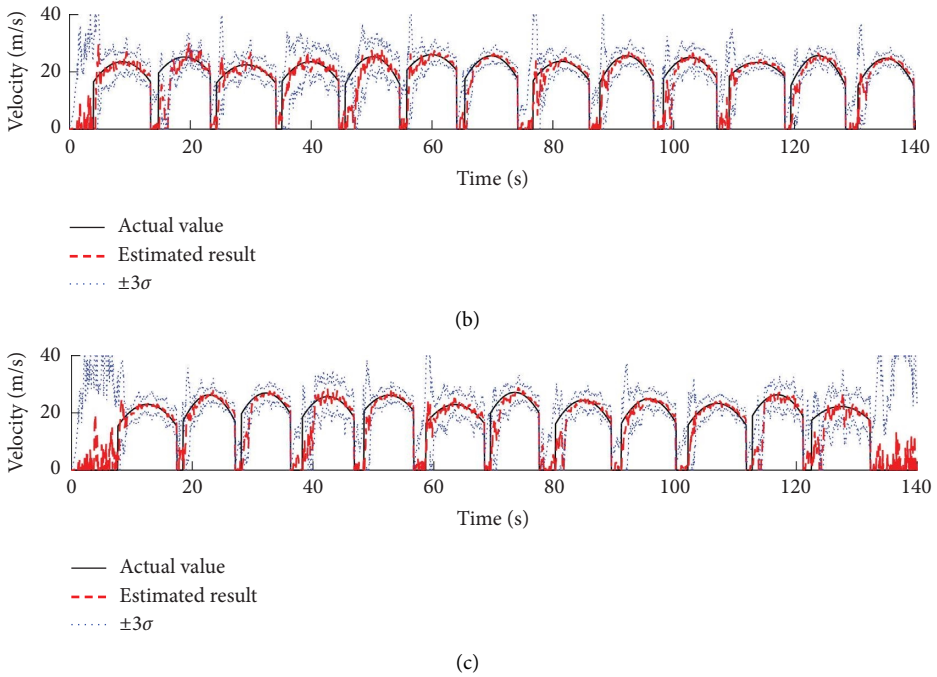


FIGURE 50: Estimated results of vehicle speeds with the proposed method: (a) first group of vehicles, (b) second group of vehicles, and (c) third group of vehicles.

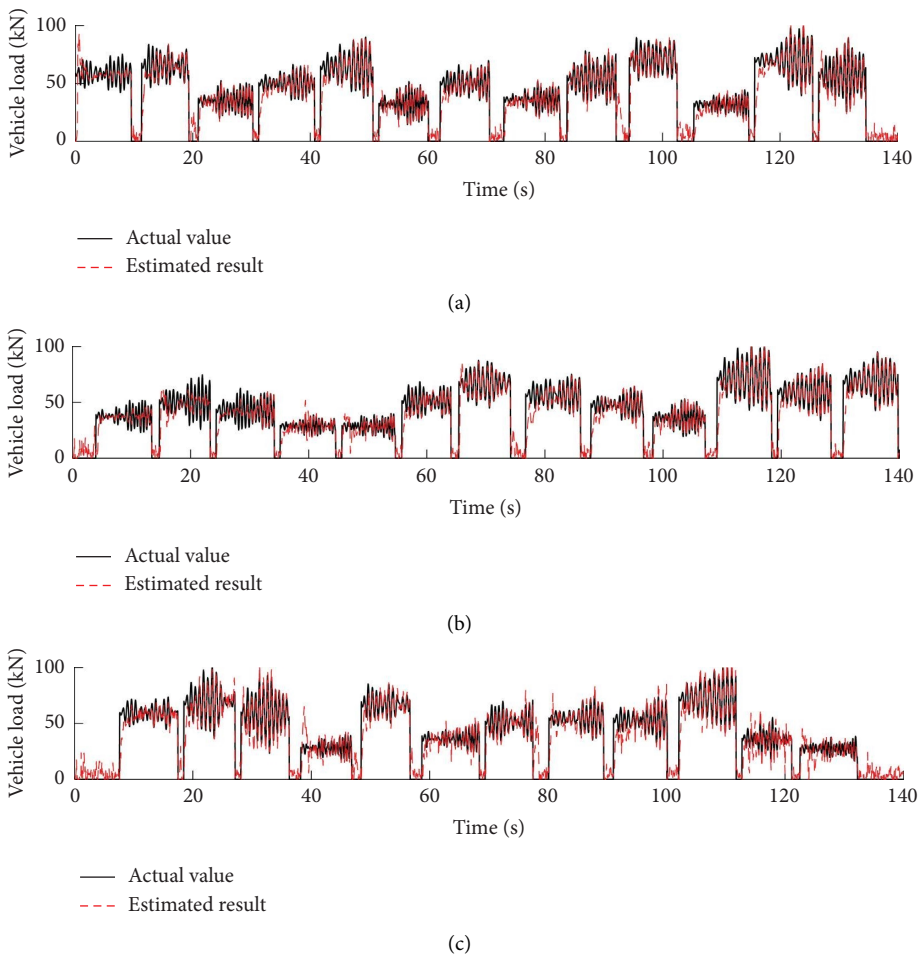


FIGURE 51: Estimated results of vehicle loads with the proposed method: (a) first group of vehicles, (b) second group of vehicles, and (c) third group of vehicles.

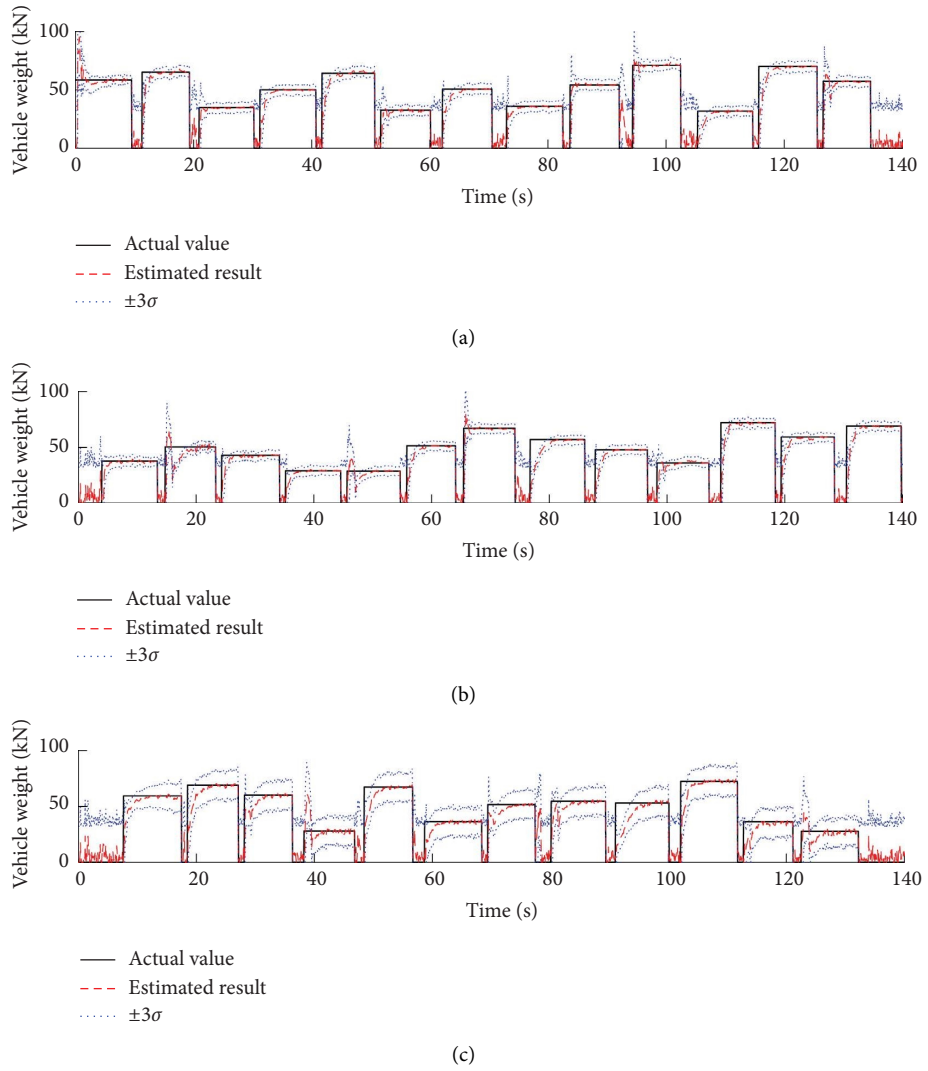


Figure 52: Estimated results of vehicle weights with the proposed method: (a) first group of vehicles, (b) second group of vehicles, and (c) third group of vehicles.

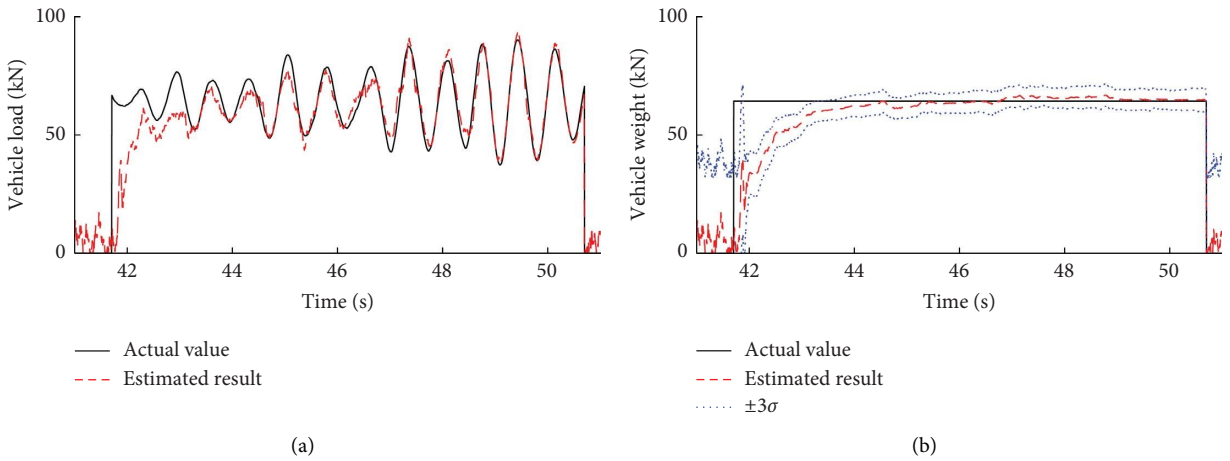


Figure 53: Estimated results of vehicle load and vehicle weight for the 13th vehicle with the proposed method: (a) vehicle load and (b) vehicle weight.

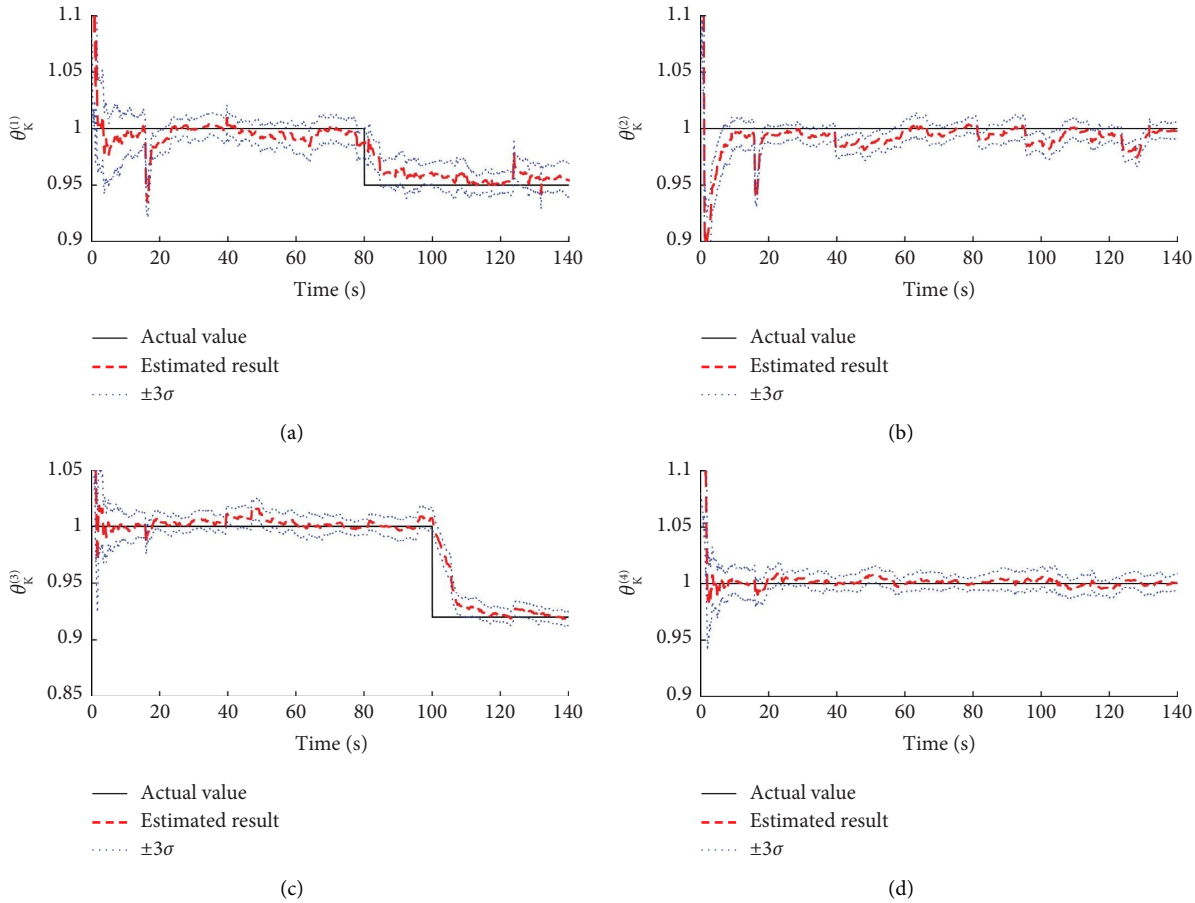


Figure 54: Estimated results of stiffness parameters with the proposed method: (a) stiffness parameter $\theta_{\mathbf{K}}^{(1)}$, (b) stiffness parameter $\theta_{\mathbf{K}}^{(2)}$, (c) stiffness parameter $\theta_{\mathbf{K}}^{(3)}$, and (d) stiffness parameter $\theta_{\mathbf{K}}^{(4)}$.

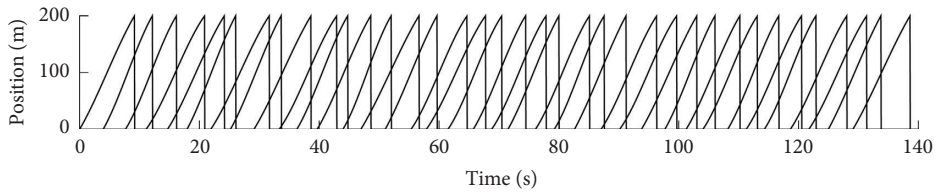


Figure 55: Time histories of vehicle positions.

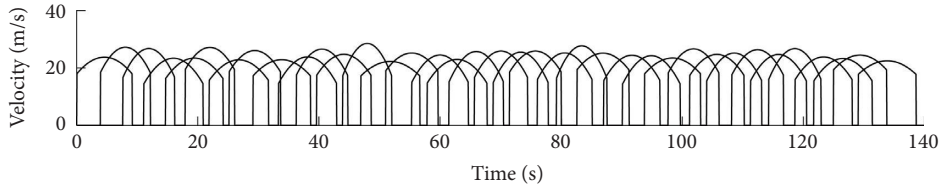


Figure 56: Time histories of vehicle speeds.

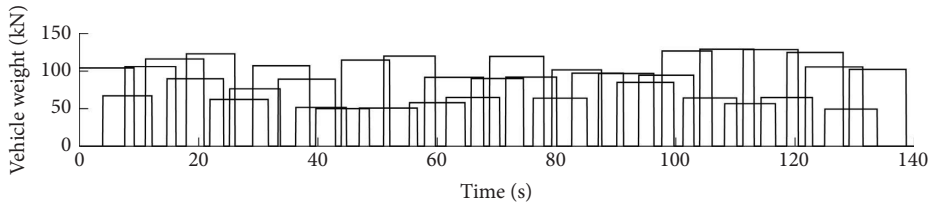


Figure 57: Time histories of vehicle weights.

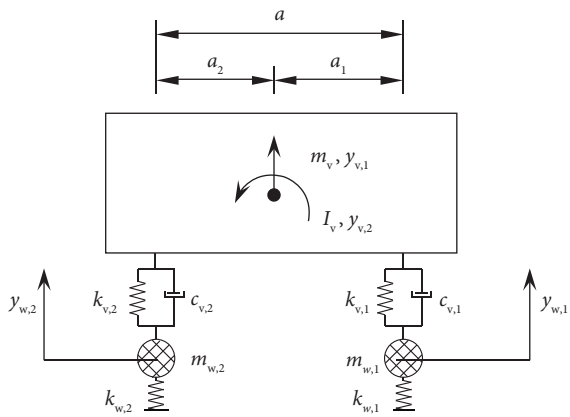


Figure 58: Two-axle vehicle model.

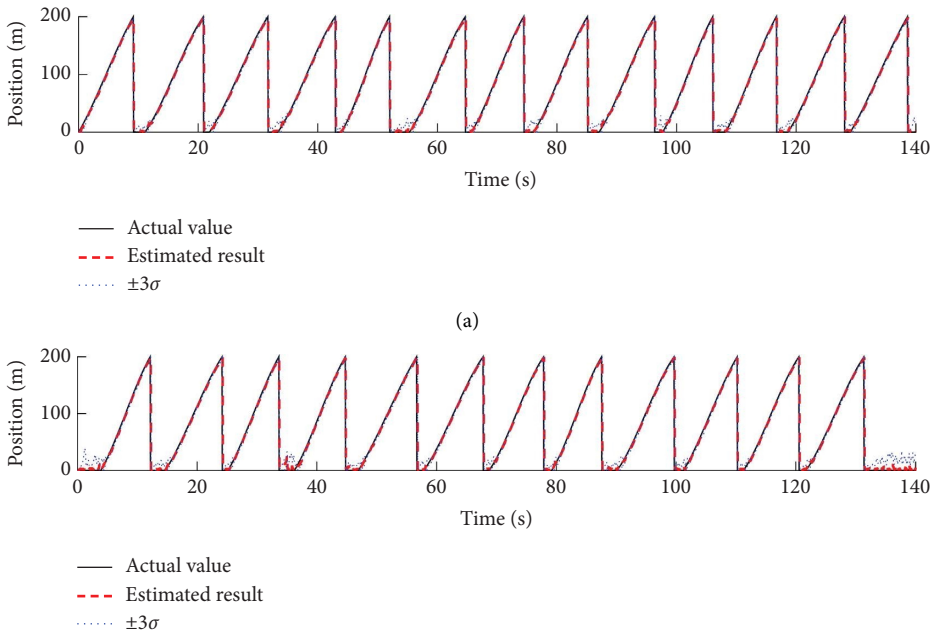


Figure 59: Continued.

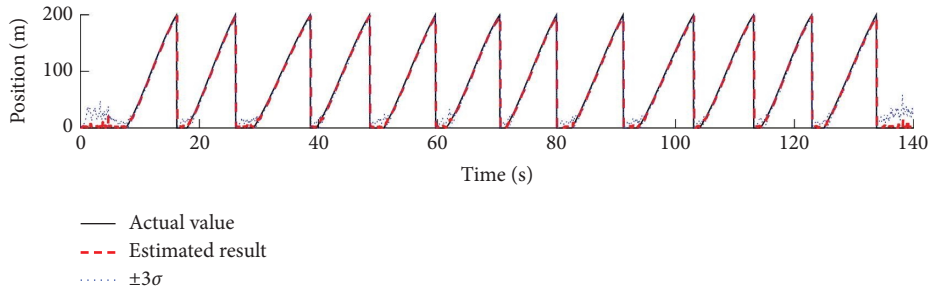


(c)

FIGURE 59: Estimated results of vehicle positions with the proposed method: (a) first group of vehicles, (b) second group of vehicles, and (c) third group of vehicles.

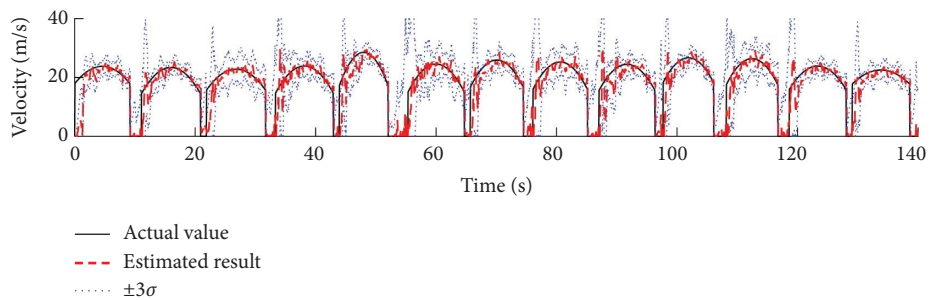


(a)

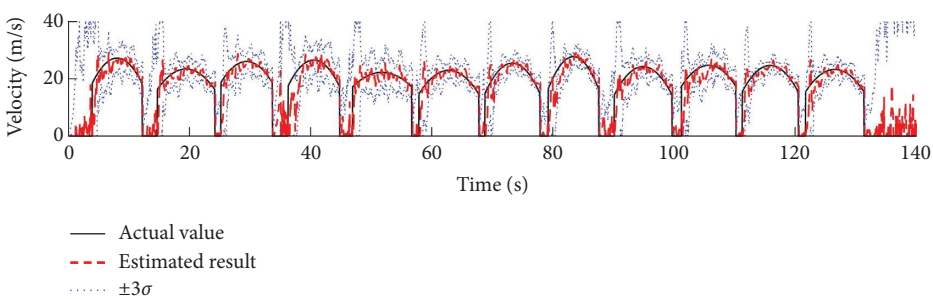


(b)

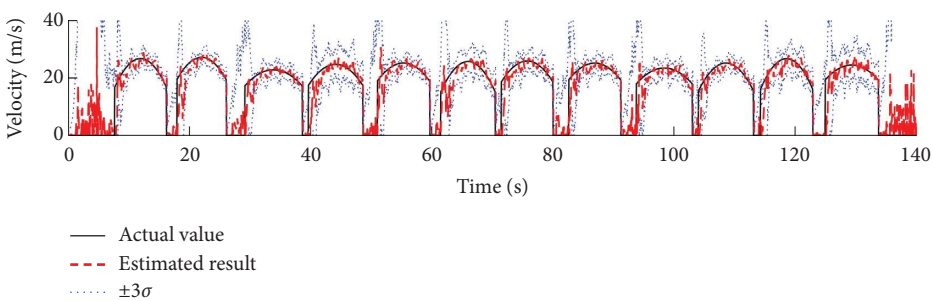


(c)

FIGURE 60: Estimated results of vehicle speeds with the proposed method: (a) first group of vehicles, (b) second group of vehicles, and (c) third group of vehicles.

$m_{v,0} = 8 \times 10^3$ kg and $I_v = 9.5 \times 10^5$ kg $\cdot$ m$^2$, respectively. The masses of the two wheels are $m_{w,1} = 7 \times 10^2$ kg and $m_{w,1} = 1.1 \times 10^3$ kg, respectively. The stiffness and the damping of the suspension system for the front wheel are $k_{v,1} = 0.40 \times 10^6$ N/m and $c_{v,1} = 1.00 \times 10^4$ N/(m/s), respectively, and the corresponding parameters for the rear wheel are $k_{v,2} = 1.00 \times 10^6$ N/m and $c_{v,2} = 2.00 \times 10^4$ N/(m/s). The stiffnesses of the two wheels are $k_{w,1} = 1.75 \times 10^6$ N/m and $k_{w,2} = 3.50 \times 10^6$ N/m, respectively. To simulate the different weights of the vehicles, the weights of

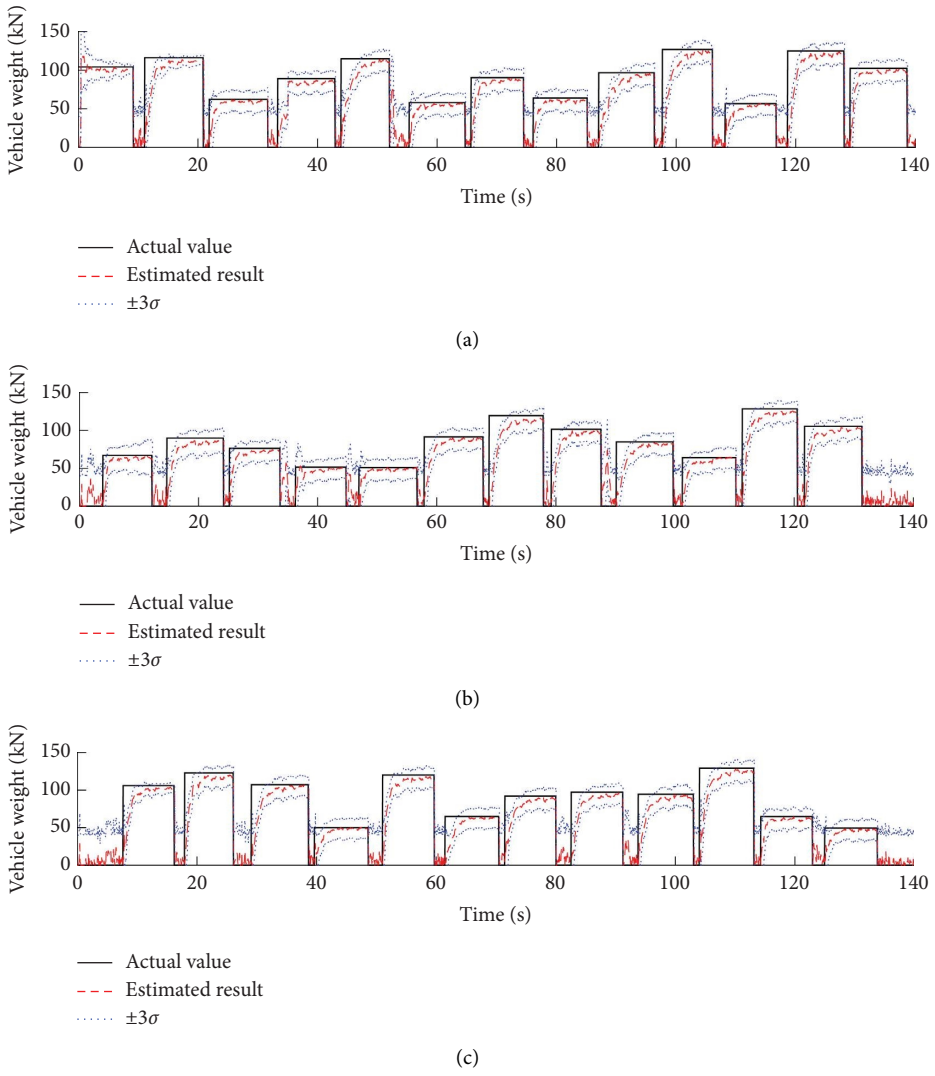


FIGURE 61: Estimated results of vehicle weights with the proposed method: (a) first group of vehicles, (b) second group of vehicles, and (c) third group of vehicles.

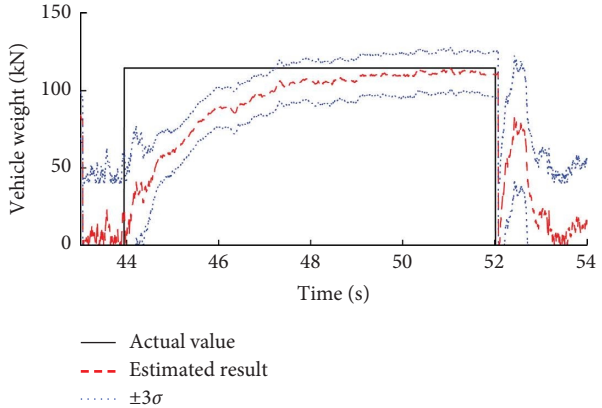


FIGURE 62: Estimated result of vehicle weight for the 13th vehicle with the proposed method.

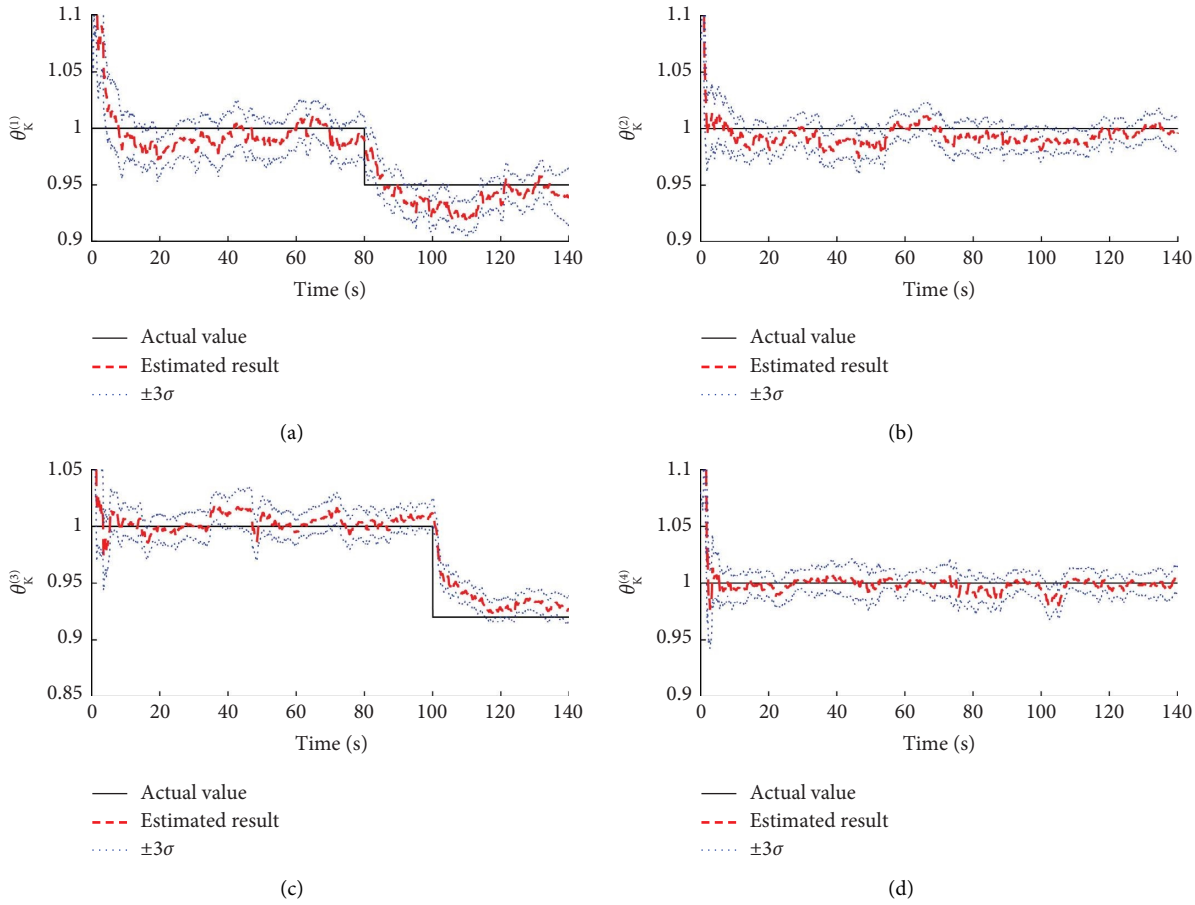


FIGURE 63: Estimated results of stiffness parameters with the proposed method: (a) stiffness parameter $\theta_{\mathbf{K}}^{(1)}$, (b) stiffness parameter $\theta_{\mathbf{K}}^{(2)}$, (c) stiffness parameter $\theta_{\mathbf{K}}^{(3)}$, and (d) stiffness parameter $\theta_{\mathbf{K}}^{(4)}$.

the vehicles are adjusted as $G = \phi_G G_0$ with $G_0 = (m_{v,0} + m_{w,1} + m_{w,2})g$ and $\phi_G \sim U(0.5,1.5)$. In this example, the maximum number of the vehicles moving on the bridge simultaneously is $N_v = 3$.

Figures 59 and 60 show the estimated results of vehicle positions and vehicle speeds. The estimated results match well with the actual values, which indicates the feasibility of the proposed method for the position tracking the vehicles. Figure 61 shows the estimated results of vehicle weights. For clarity, the magnified result for the 13th vehicle is presented in Figure 62. After the first few seconds, the vehicle weight of the 13th vehicle is well identified demonstrating that satisfactory estimation of the total weight of the vehicles can still be achieved, even though the axle configuration of a two-axle vehicle is considered. Note that the estimated results of vehicle loads are not presented since the actual loads are the axle loads of the vehicles. Figure 63 shows the estimated stiffness parameters. The estimated results make a good agreement with the actual ones.

## 6. Conclusion

In this paper, a Bayesian probabilistic approach is developed for the online estimation of vehicle loads, vehicle positions, and structural parameters of bridges using strain measurements. There are three remarkable features in the present approach. First, it allows the real-time simultaneous vehicle load estimation, vehicle position tracking, and structural identification of bridges using only strain measurements. Second, this method allows for vehicles with time-varying speeds. Third, the proposed method is applicable to the case with multiple vehicles. Two examples are presented to demonstrate the feasibility of the proposed method. Comparison with the existing methods shows the efficacy of the filtered noise model for vehicle load estimation. Estimation of the bridge structures under different vehicle passing cases validates the feasibility of the proposed methods for the simultaneous estimation of vehicle loads, vehicle positions, and structural parameters of a single-span

or multispan bridges subjected to successive vehicle loads, including successive single/multiple vehicles with different weights and uniform/variable speeds.

## Data Availability

The data used in this study are available on request from the corresponding author.

## Conflicts of Interest

The authors declare that they have no conflicts of interest.

## Acknowledgments

This work was supported by the Science and Technology Development Fund, Macau SAR (Grant SKL-IOTSC(UM)-2021-2023), University of Macau (CPG2023-00003-FST), Guangdong-Hong Kong-Macau Joint Laboratory Program (Project no. 2020B1212030009), the National Key R&D Program of China (Grant no. 2019YFC1511000), the National Natural Science Foundation of China (Grant no. 52008037), Guangdong Provincial Key Laboratory of Modern Civil Engineering Technology (2021B1212040003), and the State Key Laboratory of Internet of Things for Smart City (University of Macau) (SKL-IoTSC(UM)-2024-2026/ORP/GA07/2023); this generous support is gratefully acknowledged.

## References

[1] X. Q. Zhu and S. S. Law, "Recent developments in inverse problems of vehicle–bridge interaction dynamics," *Journal of Civil Structural Health Monitoring*, vol. 6, no. 1, pp. 107–128, 2016.

[2] M. Lydon, S. E. Taylor, D. Robinson, A. Mufti, and E. J. O. Brien, "Recent developments in bridge weigh in motion (B-WIM)," *Journal of Civil Structural Health Monitoring*, vol. 6, no. 1, pp. 69–81, 2016.

[3] Y. Yu, C. S. Cai, and L. Deng, "State-of-the-art review on bridge weigh-in-motion technology," *Advances in Structural Engineering*, vol. 19, no. 9, pp. 1514–1530, 2016.

[4] H. Sekiya, "Field verification over one year of a portable bridge weigh-in-motion system for steel bridges," *Journal of Bridge Engineering*, vol. 24, no. 7, Article ID 04019063, 2019.

[5] F. Moses, "Weigh-in-motion system using instrumented bridges," *Transportation Engineering Journal of ASCE*, vol. 105, no. 3, pp. 233–249, 1979.

[6] B. Jacob, "Weighing-in-motion of axles and vehicles for Europe (WAVE)," Rep. Of Work Package 1.2, Laboratoire Central des Ponts et Chaussees, Paris, 2001.

[7] E. J. O'Brien, D. Hajializadeh, N. Uddin, D. Robinson, and R. Opitz, "Strategies for axle detection in bridge weigh-in-motion systems," in *Proceedings of the 6th International Conference on Weigh-In-Motion (ICWIM 6)*, pp. 79–88, Wiley, Hoboken, NJ, USA, June 2012.

[8] T. F. Bao, S. K. Babanajad, T. Taylor, and F. Ansari, "Generalized method and monitoring technique for shear-strain-based bridge weigh-in-motion," *Journal of Bridge Engineering*, vol. 21, no. 1, Article ID 04015029, 2016.

[9] M. Lydon, D. Robinson, S. E. Taylor, G. Amato, E. J. O. Brien, and N. Uddin, "Improved axle detection for bridge weigh-in-motion systems using fiber optic sensors," *Journal of Civil Structural Health Monitoring*, vol. 7, no. 3, pp. 325–332, 2017.

[10] W. He, L. Deng, H. Shi, C. S. Cai, and Y. Yu, "Novel virtual simply supported beam method for detecting the speed and axles of moving vehicles on bridges," *Journal of Bridge Engineering*, vol. 22, no. 4, Article ID 04016141, 2017.

[11] W. He, T. Y. Ling, E. J. O'Brien, and L. Deng, "Virtual axle method for bridge weigh-in-motion systems requiring no axle detector," *Journal of Bridge Engineering*, vol. 24, no. 9, Article ID 04019086, 2019.

[12] S. S. Law and X. Q. Zhu, *Moving Loads-Dynamic Analysis and Identification Techniques*, CRC Press, Taylor & Francis Group, London, 2011.

[13] H. Ouyang, "Moving-load dynamic problems: a tutorial (with a brief overview)," *Mechanical Systems and Signal Processing*, vol. 25, no. 6, pp. 2039–2060, 2011.

[14] T. Ojio and K. Yamada, "Bridge weigh-in-motion systems using stringers of plate girder bridges," in *Proceedings of the 3rd International Conference on Weigh-In-Motion (IC-WIM 3)*, pp. 209–218, FHWA, Orlando, FL, USA, August 2002.

[15] S. S. Law, T. H. T. Chan, and Q. H. Zeng, "Moving force identification: a time domain method," *Journal of Sound and Vibration*, vol. 201, no. 1, pp. 1–22, 1997.

[16] T. H. T. Chan, S. S. Law, and T. H. Yung, "Moving force identification using an existing pre-stressed concrete bridge," *Engineering Structures*, vol. 22, no. 10, pp. 1261–1270, 2000.

[17] H. Sun and O. Büyüköztürk, "Identification of traffic-induced nodal excitations of truss bridges through heterogeneous data fusion," *Smart Materials and Structures*, vol. 24, no. 7, Article ID 075032, 2015.

[18] D. M. Feng, H. Sun, and M. Q. Feng, "Simultaneous identification of bridge structural parameters and vehicle loads," *Computers & Structures*, vol. 157, pp. 76–88, 2015.

[19] Z. Chen, T. H. T. Chan, and L. Yu, "Comparison of regularization methods for moving force identification with ill-posed problems," *Journal of Sound and Vibration*, vol. 478, Article ID 115349, 2020.

[20] X. Kong, J. Zhang, T. Y. Wang, L. Deng, and C. S. Cai, "Non-contact vehicle weighing method based on tire-road contact model and computer vision techniques," *Mechanical Systems and Signal Processing*, vol. 174, Article ID 109093, 2022.

[21] R. Lalthlamuana and S. Talukdar, "Estimation of gross weight, suspension stiffness and damping of a loaded truck from bridge measurements," *Structure and Infrastructure Engineering*, vol. 13, no. 11, pp. 1497–1512, 2017.

[22] H. Q. Wang, T. Nagayama, B. Y. Zhao, and D. Su, "Identification of moving vehicle parameters using bridge responses and estimated bridge pavement roughness," *Engineering Structures*, vol. 153, pp. 57–70, 2017.

[23] H. Q. Wang, T. Nagayama, and D. Su, "Static and dynamic vehicle load identification with lane detection from measured bridge acceleration and inclination responses," *Structural Control and Health Monitoring*, vol. 28, no. 11, pp. 1–21, 2021.

[24] M. Doumiati, A. Charara, A. Victorino, and D. Lechner, *Vehicle Dynamics Estimation Using Kalman Filtering: Experimental Validation*, John Wiley & Sons, Hoboken, NJ, USA, 2012.

[25] X. G. Lai, M. Furkan, I. Bartoli, A. E. Aktan, and K. Grimmelsman, "Bridge weigh-in-motion using augmented Kalman filter and model updating," *Journal of Civil Structural Health Monitoring*, vol. 12, no. 3, pp. 593–610, 2022.

[26] T. Ojio, C. H. Carey, E. J. O'Brien, C. Doherty, and S. E. Taylor, "Contactless bridge weigh-in-motion," *Journal of Bridge Engineering*, vol. 21, no. 7, Article ID 04016032, 2016.

[27] A. Lansdell, W. Song, and B. Dixon, "Development and testing of a bridge weigh-in-motion method considering nonconstant vehicle speed," *Engineering Structures*, vol. 152, pp. 709–726, 2017.

[28] S. Z. Chen, G. Wu, D. C. Feng, and L. Zhang, "Development of a bridge weigh-in-motion system based on long-gauge fiber Bragg grating sensors," *Journal of Bridge Engineering*, vol. 23, no. 9, Article ID 04018063, 2018.

[29] S. Z. Chen, G. Wu, and D. C. Feng, "Development of a bridge weigh-in-motion method considering the presence of multiple vehicles," *Engineering Structures*, vol. 191, pp. 724–739, 2019.

[30] G. Yang, S. Z. Chen, X. Y. Wang, and D. Hu, "Study on data-driven identification method of hinge joint damage under moving vehicle excitation," *ASCE-ASME Journal of Risk and Uncertainty in Engineering Systems, Part A: Civil Engineering*, vol. 9, no. 4, Article ID 04023035, 2023.

[31] Z. Chen, H. Li, Y. Bao, N. Li, and Y. Jin, "Identification of spatio-temporal distribution of vehicle loads on long-span bridges using computer vision technology," *Structural Control and Health Monitoring*, vol. 23, no. 3, pp. 517–534, 2016.

[32] A. Moghadam, M. AlHamaydeh, and R. Sarlo, "Bridge-weigh-in-motion approach for simultaneous multiple vehicles on concrete-box-girder bridges," *Automation in Construction*, vol. 137, Article ID 104179, 2022.

[33] T. M. Deepthi, U. Saravanan, and A. M. Prasad, "Algorithms to determine wheel loads and speed of trains using strains measured on bridge girders," *Structural Control and Health Monitoring*, vol. 26, no. 1, pp. 1–26, 2019.

[34] M. Sujon and F. Dai, "Application of weigh-in-motion technologies for pavement and bridge response monitoring: state-of-the-art review," *Automation in Construction*, vol. 130, Article ID 103844, 2021.

[35] Z. Chen, L. F. Qin, T. H. T. Chan, and L. Yu, "A novel preconditioned range restricted GMRES algorithm for moving force identification and its experimental validation," *Mechanical Systems and Signal Processing*, vol. 155, Article ID 107635, 2021.

[36] Y. B. Yang, J. D. Yau, and Y. S. Wu, *Vehicle-bridge Interaction Dynamics: With Applications to High-Speed Railways*, World Scientific Publishing Co, Singapore, 2004.

[37] K. L. Johnson, *Contact Mechanics*, Cambridge University Press, Cambridge, UK, 1985.

[38] K. V. Yuen and K. Huang, "Real-time substructural identification by boundary force modeling," *Structural Control and Health Monitoring*, vol. 25, no. 5, Article ID e2151, 2018.

[39] K. Huang, K. V. Yuen, and L. Wang, "Real-time simultaneous input-state-parameter estimation with modulated colored noise excitation," *Mechanical Systems and Signal Processing*, vol. 165, Article ID 108378, 2022.

[40] R. E. Kalman, "A new approach to linear filtering and prediction problems," *Journal of Basic Engineering*, vol. 82, no. 1, pp. 35–45, 1960.

[41] J. N. Yang, S. Pan, and H. Huang, "An adaptive extended Kalman filter for structural damage identifications II: unknown inputs," *Structural Control and Health Monitoring*, vol. 14, no. 3, pp. 497–521, 2007.

[42] H. Huang, J. N. Yang, and L. Zhou, "Adaptive quadratic sum-squares error with unknown inputs for damage identification of structures," *Structural Control and Health Monitoring*, vol. 17, no. 4, pp. 404–426, 2010.

[43] H. Q. Mu and K. V. Yuen, "Novel outlier-resistant extended Kalman filter for robust online structural identification," *Journal of Engineering Mechanics*, vol. 141, no. 1, Article ID 04014100, 2015.

[44] K. V. Yuen and H. Q. Mu, "Real-time system identification: an algorithm for simultaneous model class selection and parametric identification," *Computer-Aided Civil and Infrastructure Engineering*, vol. 30, no. 10, pp. 785–801, 2015.

[45] K. V. Yuen and S. C. Kuok, "Online updating and uncertainty quantification using nonstationary output-only measurement," *Mechanical Systems and Signal Processing*, vol. 66, pp. 62–77, 2016.

[46] H. Q. Mu, S. C. Kuok, and K. V. Yuen, "Stable robust extended Kalman filter," *Journal of Aerospace Engineering*, vol. 30, no. 2, Article ID B4016010, 2017.

[47] J. Q. Li, X. L. Leng, and T. Fang, "Evolutionary random response problem of a coupled vehicle-bridge system," *Archive of Applied Mechanics*, vol. 72, no. 6-7, pp. 536–544, 2002.

[48] M. Shinozuka and G. Deodatis, "Stochastic process models for earthquake ground motion," *Probabilistic Engineering Mechanics*, vol. 3, no. 3, pp. 114–123, 1988.